Petroleum Science 22 (2025) 557–573

Contents lists available at ScienceDirect

Petroleum Science

journal homepage: www.keaipublishing.com/en/journals/petroleum-science

Original Paper

Pore formation and evolution mechanisms during hydrocarbon generation in organic-rich marl

Tong Wang [a], Xiao-Feng Wang [a], Dong-Dong Zhang [a], Qing-Tao Wang [b], Hou-Yong Luo [a], Jie Wang [c], Zhong-Liang Ma [c], Zhang-Xing Chen [d, e], Wen-Hui Liu [a, f, *]

[a] State Key Laboratory of Continental Dynamics, Department of Geology, Northwest University, Xi'an, 710069, Shaanxi, China
[b] School of Mechatronic Engineering, Guangdong Polytechnic Normal University, Guangzhou, 510665, Guangdong, China
[c] Wuxi Research Institute of Petroleum Geology, SINOPEC, Wuxi, 214126, Jiangsu, China
[d] Easter Institute of Technology, Ningbo, 315200, Zhejiang, China
[e] Department of Chemical and Petroleum Engineering, University of Calgary, Calgary, Alberta, T2N 1N4, Canada
[f] Petroleum Exploration □ Production Research Institute, SINOPEC, Beijing, 100083, China

ARTICLE INFO

Article history:
Received 28 April 2024
Received in revised form
13 July 2024
Accepted 31 October 2024
Available online 2 November 2024

Edited by Jie Hao

Keywords:
Organic-rich marl
Hydrocarbon generation-expulsion-retention process
OM pores
Pore evolution
Organic-inorganic interactions

ABSTRACT

Marine organic-rich marl is not only a high-quality hydrocarbon source of conventional oil and gas, but also a new type and field of unconventional oil and gas exploration. An understanding of its pore structure evolution characteristics during a hydrocarbon generation process is theoretically significant and has application prospects for the exploration and development of this special type of natural gas reservoirs. This study conducted thermal simulation of hydrocarbon generation under near-geological conditions during a whole process for cylinder samples of low mature marine organic-rich marl in the Middle Devonian of Luquan, Yunnan Province, China. During this process, hydrocarbon products at different evolution stages were quantified and corresponding geochemical properties were analyzed. Simultaneously, field emission scanning electron microscopy (FE-SEM) and low-pressure gas adsorption (CO_2, N_2) tests were applied to the corresponding cylinder residue samples to reveal the mechanisms of different types of pore formation and evolution, and clarify the dynamic evolution processes of their pore systems. The results show that with an increase in temperature and pressure, the total oil yield peaks at an equivalent vitrinite reflectance (VR_o) of 1.03% and is at the maximum retention stage of liquid hydrocarbons, which are 367.51 mg/g TOC and 211.67 mg/g TOC, respectively. The hydrocarbon gas yield increases continuously with an increase in maturity. The high retained oil rate at the peak of oil generation provides an abundant material basis for gas formation at high maturity and over-maturity stage. The lower limit of VR_o for organic matter (OM) pore mass development is about 1.6%, and bitumen pores, organic-clay complex pores together with intergranular pores, grain edge seams and dissolution pores constitute a complicated pore-seam-network system, which is the main reservoir space for unconventional carbonate gas. Pore formation and evolution are controlled synergistically by hydrocarbon generation, diagenesis and organic-inorganic interactions, and the pattern of pore structure evolution can be divided into four stages. A pore volume (PV) and a specific surface area (SSA) are at their highest values within the maturity range of 1.9% to 2.5%, which is conducive to exploring unconventional natural gas.

1. Introduction

North America's shale gas and China's southern marine shale gas exploration and development have major breakthroughs successively, which have drawn the attention of many scholars around the world to the geological research of unconventional oil and gas resources (Jarvie, 2012; Ko et al., 2018; Zou et al., 2018; Dong et al., 2019). Organic-rich shales and fine-grained carbonates are the main hydrocarbon source rock types of marine shale gas in southern China. At present, the Wufeng Formation and Longmaxi Formation marine shale gas resources in the Sichuan basin in China

* Corresponding author. State Key Laboratory of Continental Dynamics, Department of Geology, Northwest University, Xi'an, 710069, Shaanxi, China.
E-mail address: whliu@nwu.edu.cn (W.-H. Liu).

https://doi.org/10.1016/j.petsci.2024.10.011

have been realized with commercial development and have enormous potential for exploration. Recently, the source-reservoir integration marine marl oil and gas resources have obtained high-yield industrial gas flow in the Permian Maokou formation and Triassic Leikoupo formation in the Sichuan basin, which further confirms that a marl system can be used as both a hydrocarbon source rock for conventional hydrocarbons and a reservoir for unconventional hydrocarbons (Su et al., 2021; Wang et al., 2023b). However, the mechanisms of pore formation and evolution in organic-rich marl are still unclear, constraining the exploration and deployment of this new type of natural gas.

The pore structure characteristics of organic-rich rocks not only affect an occurrence state and seepage capacity of hydrocarbons, but also are the key factors for controlling hydrocarbon accumulation and enrichment. Many scholars have qualitatively described and quantitatively characterized the pore sizes, morphology, and connectivity of organic-rich shale using FE-SEM, Nano CT, nuclear magnetic resonance, low-temperature gas adsorption and high-pressure mercury injection (Loucks et al., 2012; Lai et al., 2018; Ren et al., 2019; Qin et al., 2022). It is widely recognized that the OM pores of high-mature marine shale are relatively developed, which is the primary reservoir space for marine shale gas. Meanwhile, shale nano-scale OM pore development has variability, which is mainly influenced by factors such as total organic carbon (TOC), thermal maturity (R_o), an OM type, and mineralogical composition (Jarvie et al., 2007; Gao et al., 2020). Currently, most scholars analyze the mechanism of pore formation and evolution by investigating the pore structure characteristics of naturally evolving shale samples with different values of R_o in a same region, and establishing related porosity evolution models (Dong et al., 2019; Mastalerz et al., 2013; Milliken et al., 2013; Sarmiento et al., 2014). However, because of the extreme heterogeneity of organic-rich fine-grained sedimentary rocks, the mineral composition, microscopic structure, and OM content of samples taken from different depths of a same geologic section can vary greatly. Therefore, conflicting conclusions are obtained by different experts for a same research purpose. A hydrocarbon generation simulation experiment is a key means to characterize the processes of hydrocarbon generation, expulsion and retention in hydrocarbon source rocks. Over the past few years, scholars have used hydrocarbon generation simulation experimental devices to artificially heat immature or low-mature source rock samples to different thermal evolution stages, and then applied multi-method testing techniques to characterize the evolution of pore structure (Chen and Xiao, 2014; Wang and Guo, 2019; Wu et al., 2019; Guo et al., 2020). This method can not only effectively avoid the problem of heterogeneity of samples, but also realizes a “dynamic” evolution process of the pore structure.

For a long time, the target strata for marine shale gas exploration in southern China are mainly organic-rich siliceous shale, calcareous shale and clayey shale. Organic-rich marl is only treated as a carbonate hydrocarbon source rock, and too much attention has been paid to the quality of its hydrocarbon source while overlooking as a reservoir for research. With the breakthrough of source-reservoir integration marl oil and gas exploration, researchers have begun to focus on a relationship between a retention space and the evolution of hydrocarbon generation-expulsion-retention (Wang et al., 2023c). Notably, most scholars have confirmed and recognized that OM hydrocarbon generation and inorganic diagenesis synergistically control the formation and evolution of a pore structure in organic-rich mud shale reservoirs (Shao et al., 2020; Song et al., 2020a; Xu et al., 2021; Cao et al., 2021). However, due to different depositional environments and diagenetic processes, the pore structure of organic-rich marl is more complicated than that of shale, which is mainly reflected in (1) different states of OM enrichment: besides granular OM, organic acid salts are also important sources of hydrocarbons in organic-rich marl (Liu et al., 2017) and additionally, it is also common to observe OM complicated with clay minerals in the form of organic-clay complexes (Wang et al., 2023a; Zhu et al., 2020); (2) different mineral frameworks of source rocks: marl has a higher content of rigid minerals such as calcite, which is resistant to compaction and provides important support and preservation for OM pores (Borjigin et al., 2021); (3) organic-inorganic interactions are more extensive. Acidic fluids generated during OM generation-expulsion processes are more likely to react with carbonate minerals, which form dissolved pores and increase a pore space (Xu et al., 2021). Furthermore, pore spaces associated with organic-clay complexes are more easily exposed in a high maturity stage because of the massive decomposition of OM. Therefore, a pore development mechanism and prediction are difficult and key points in the study of marine carbonate unconventional gas reservoirs.

In this paper, semi-open hydrous pyrolysis simulation experiments under near-geological conditions were carried out on the same horizontal layers of low-maturity marl cylinder samples, with simulated temperatures covering the stage of hydrocarbon generation evolution from low maturity to over-maturity (VR_o ranging from 0.55% to 3.55%). This paper focuses on the synergistic evolution of reservoir space and hydrocarbon generation-expulsion-retention in marine organic-rich marl, which aims to reveal the mechanisms of different types of pore formation and evolution, as well as to provide a theoretical basis and a research method for the exploration of unconventional oil and gas resources in the marine carbonate rocks in southern China.

2. Samples and methods

2.1. Sample information

The experimental samples were collected from the profile of Jianshangcun, Huaning Formation, Middle Devonian, Luquan area, Yunnan Province, China, which is located next to the Chu Xiong Basin of the Upper Yangzi Plate, with the specific GPS location of N 25° 39′ 52″, E 102° 31′ 44″ (Fig. 1). There are mainly dark-gray marl, gray-black marl and calcareous mudstone developed in the profile. Previous studies (Ma et al., 2020, 2021) revealed that the sedimentary environment of the sample was strong reduction-reduction conditions, and the main hydrocarbon forming organisms were algae and low aquatic organisms, as well as the contribution of certain terrestrial plants, with strong hydrocarbon generation potential.

Original sample TOC and VR_o were 6.13% and 0.51%, respectively. Basic organic geochemical parameters of the samples are shown in Table 1, with cracked hydrocarbons (S_2) and hydrogen index (HI) of 25.47 mg/g and 439 mg/g TOC, respectively. The HI -Tmax plot shows that the organic matter type is typical of Type II_1 (Fig. 2). XRD analysis results indicate that calcite (66.8%), clay minerals (15.9%), and quartz (13.1%) are the dominant mineral composition (Table 2). In summary, the study samples are low-mature marine organic-rich marls dominated by type II_1 kerogen, which are the ideal samples for hydrocarbon generation simulation experiments.

2.2. Experimental procedures and methods

Given the heterogeneity of the carbonate rock, during the preprocessing of the samples, we drilled 12 cylindrical cores with a diameter of about 25 mm on the same large organic matter-rich marl sample using a core drilling rig. The cores were vertical to the horizontal bedding plane, with the distance between adjacent cores less than 2 cm to minimize the influence of OM heterogeneity

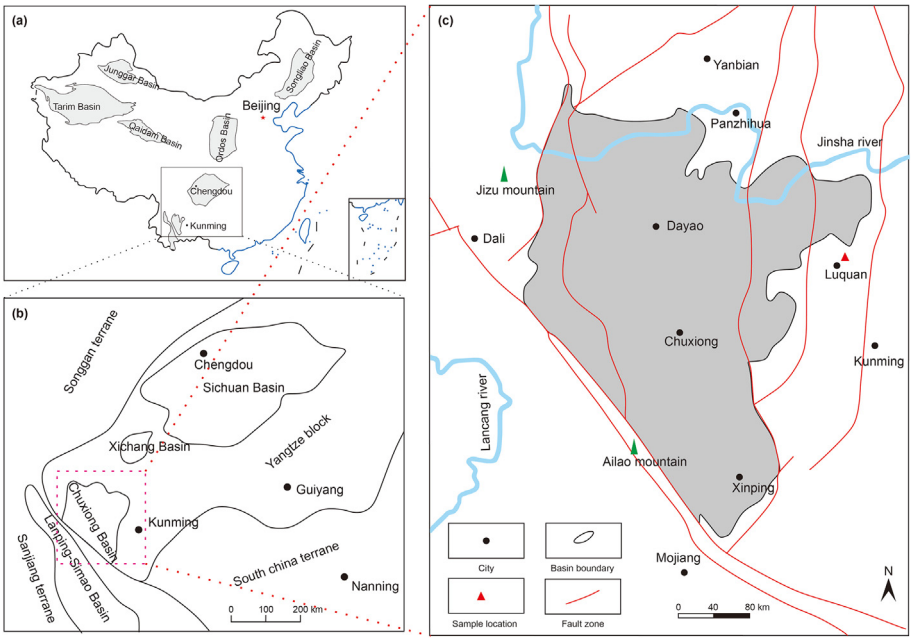

Fig. 1. Tectonic location and geographic location of simulated experimental samples. **(a)** Tectonic location; **(b)** study area; **(c)** sampling location.

Table 1
Basic organic geochemical data for experimental samples.

Sample	TOC, %	R_b, %	VR_o, %	T_{max}, °C	HI, mg/g TOC	OI, mg/g TOC	S_1, mg/g	S_2, mg/g
LQ-O	6.13	0.46	0.51	432	439	7	2.2	25.47

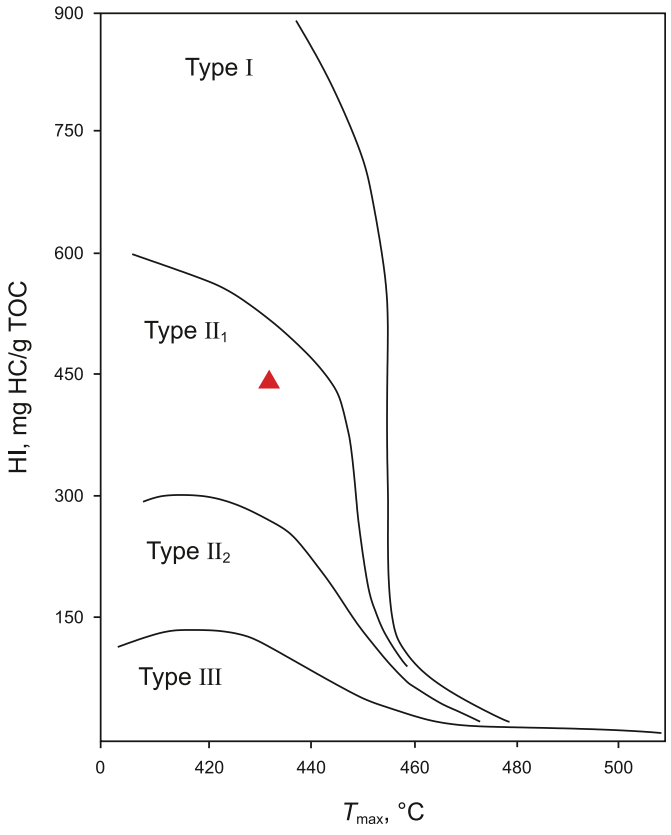

Fig. 2. OM type determination chart.

on the results of hydrocarbon generation simulation experiments (Fig. 3). The detailed experimental design and analysis procedures can be seen in Fig. 4.

2.2.1. Semi-closed system hydrous pyrolysis simulation experiments

The semi-closed system hydrous pyrolysis simulation experiment was completed by using the DK-IV formation pore thermal pressure hydrocarbon simulation instrument of the Wuxi Institute of Petroleum and Geology, SINOPEC. Different from other semi-closed system pyrolysis experiments, this instrument is capable of simultaneously applying overlying lithostatic rock pressure, surrounding pressure, and formation fluid pressure values that are close to the geologic burial conditions to the simulated samples under high temperature conditions. Secondly, the hydrocarbons generated from the source rock are “episodic expulsion” under a certain condition of pressure difference, that is, generation of hydrocarbons and expulsion of hydrocarbons at the same time. In addition, the samples are cylindrical cores, which retain the microstructure of source rock samples and the state of OM.

Simulation experiments use the actual burial history and thermal evolution history of typical wells in the southeastern Sichuan Basin as geological constraint boundary conditions (Qiu et al., 2022). The experimental design scheme is shown in Table 3. The heating program was from room temperature to the target temperature at a rate of 1 °C/min, followed by a constant temperature for 72 h. After loading the samples and before starting the experiment, the equipment needs to be checked for leaks, and then it was injected with formation water to ensure that the hydrocarbon space of the core samples is fully occupied. Finally, the experiment was conducted according to the pre-designed scheme until the temperature of the reaction vessel was reduced to about 150°, where the collection and quantification of gaseous products and

Table 2
Mineral composition of thermal simulation samples.

Sample	Quartz, %	Feldspar,%	Carbonate, %	Pyrite, %	Dolomite, %	Clays, %	Siderite, %	Gypsum, %	Anhydrite, %
LQ-Y	13.1	0.6	66.8	1.8	0.6	15.9	0.8	0.2	0.2

Fig. 3. Pre-prepared cylindrical core samples.

expelled oils began. A more detailed description of the device and experimental procedures can be found in (Song et al., 2019; Liu et al., 2021; Ma et al., 2021). Retained oil was quantified by measuring the chloroform bitumen "A" obtained by extracting the solid residue with dichloromethane at the end of the experiment.

2.2.2. FE-SEM and SEM experiments

Prior to the observation of the pore development characteristics of the study samples using FE-SEM, advanced pre-processing is required for the samples. Firstly, a small piece of about 1 cm * 0.7 cm * 0.7 cm in size was obtained from the target sample vertically in the bedding plane. Then, one end of the sample was mechanically smoothed and fixed on the sample platform with glue, and the other end was finely ground with diamond polishing pads of 9, 2 and 0.5 μm to remove more than 65, 25 and 6 μm on the sample surface. Polished samples were smooth and bright without visible bumps. Next, the samples were fixed on the Leica EM TIC 3X triple-ion beam cutter and vacuumed, followed by 6 rounds of 2 h argon ion beam polishing treatment alternately at 6, 5.5, 5 and 2.0 kV accelerating voltages, respectively. To further enhance the image observation quality, an approximately 2.5 nm thick carbon film was coated on the surface of the polished samples. Finally, the pore structure features of the original samples and pyrolysis samples at different simulation temperatures were observed and compared in the mode of backscattering (BSE) and secondary electron (SE) integration. In addition, the SEM observation of fresh sections of some pyrolysis samples was carried out in this study to provide a more comprehensive characterization of the pore morphology.

2.2.3. Low pressure gas adsorption test

Low-pressure gas adsorption experiments were carried out on

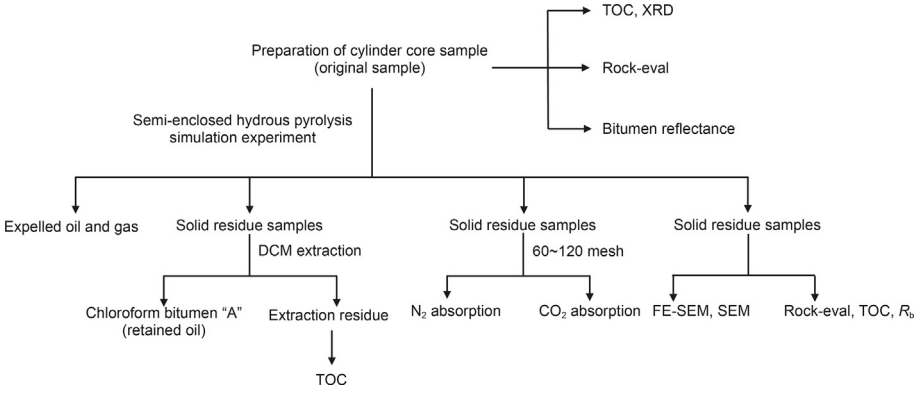

Fig. 4. Experimental design and analytical procedures (DCM refer to dichloromethane organic solvent; R_b refers to bitumen reflectance).

Table 3
Experimental scheme for the hydrocarbon generation simulation of marine organic-rich marl under near-geological conditions.

Sample ID	Simulated temperature, °C	Constant temperature time, h	Simulated burial depth, m	Lithostatic pressure, MPa	Minimum formation pressure, MPa	Maximum formation pressure, MPa	VR_o, %
LQ-275	275	72	2800	67.2	28	30.8	0.55
LQ-300	300	72	3200	76.8	32	35.2	0.61
LQ-325	325	72	3700	88.8	37	40.7	0.76
LQ-350	350	72	4500	112.5	45	49.5	1.03
LQ-375	375	72	4900	122.5	49	53.9	1.60
LQ-400	400	72	5050	126.25	50.5	55.55	1.93
LQ-425	425	72	5300	132.5	53	58.3	2.18
LQ-450	450	72	5700	142.5	57	62.7	2.47
LQ-500	500	72	6200	155	62	68.2	2.99
LQ-550	550	72	6700	167.5	67	73.7	3.55

original samples, pyrolysis samples at different simulated temperatures using a TriStar II 3020 specific surface area and pore size analyzer. Pore size classification criteria are mainly based on the IUPAC classification (Sing et al., 1985). CO_2 adsorption was used to characterize the micropore structure (<2 nm), and N_2 adsorption was used to characterize the mesopore (2–50 nm) and some macropore (50–400 nm) structures. The N_2 adsorption was performed at the saturation temperature of liquid nitrogen 77.35 K and relative pressure between 0.149 and 0.996. CO_2 adsorption tests were performed at the liquid CO_2 saturation temperature 273.15 K and relative pressure between 0.00008 and 0.037. Density Functional Theory has been applied to calculate the PV, SSA and pore size distribution (PSD) of the micropore. The Barrett-Joyner-Halenda model has been applied to analyze the PV, SSA and PSD of the mesopore and some of the macropores.

2.2.4. Organic geochemical analysis

TOC was measured on a CS744 instrument, which required complete removal of inorganic carbon from the sample with dilute hydrochloric acid before measurement. The Rock-Eval 6 rock pyrolysis instrument was operated at a temperature of 25 °C/min from 300 °C (duration 3 min) to 650 °C (duration 0 min), with further calculation and analysis to obtain the hydrocarbon source rock evaluation parameters. A classical Soxhlet extraction apparatus was utilized to extract residue samples that were ground to a particle size of 0.178 mm or less for 72 h to quantify chloroform bitumen "A" in the rock. The organic solvent used for extraction was pure dichloromethane, which was heated at a temperature not higher than 85 °C over the entire process. Due to the lack of vitrinite in the Lower Paleozoic marine source rock samples, the VR_o of the pyrolyzed samples was obtained by measuring the R_b of the samples and then transforming it into the formula "$VR_o=(R_b+0.03)/0.96$" as proposed by Bertrand (1990).

3. Result

3.1. Process of hydrocarbon generation-expulsion-retention

Hydrocarbon yield evolution at different thermal simulation experiment temperatures is shown in Fig. 5. The results show that with the increase of simulation experiment temperature, the total oil yield of the samples shows a trend of increasing, then decreasing and then leveling off, and the overall evolution trend of expelled oil and retained oil is more consistent with the total oil. At the simulated temperature increased to 350 °C with VR_o of 1.03%, the peak of oil generation was reached, as well as the peak of retained oil, corresponding to a yield of 367.51 mg/g TOC and 211.67 mg/g TOC, respectively, with roughly 57.6% of the oil still retained in the source rock system. Differently, the retained oil yield continued to decrease after reaching the peak until it approached zero after a VR_o of 2.99%; however, the expelled oil yield basically remained stable in the range of 110 mg/g TOC to 120 mg/g TOC after reaching the peak and reduced to a VR_o of 2.2%. In particular, the simulated temperature corresponding to the peak of expelled oil is higher than that of the peak of retained oil. This indicates that the large amount of generated liquid hydrocarbons expelled from the inside of the source rock must satisfy the adsorption of their kerogen itself, and the trend results coincide with those of (Hou et al., 2021; Wang et al., 2023c). In addition, the hydrocarbon gas yield increases continuously with the increases of VR_o, and the high evolution stage organic acid salts may still have some contribution.

3.2. Organic geochemical characteristics of pyrolysis residues

The organic geochemical characteristics of the pyrolysis residue samples are shown in Table 4 and Fig. 6. With the increase of temperature and pressure in the simulation experiment, TOC and HI values of the pyrolysis samples showed a gradually decreasing trend. TOC values varied from 6.13% for the original samples to 2.79% at the simulated temperature of 550 °C, with a TOC conversion rate up to 54.5%, which was caused by the thermal degradation of OM and hydrocarbon expulsion (Huang et al., 2023). Within the 375–450 °C interval, there is a certain increase in TOC content, which is mainly attributed to the generation of pyrobitumen and dead carbon. The HI from 415 mg/g TOC for the original sample to 39 mg/g TOC at the simulated temperature of 400 °C consumed 90% of the hydrocarbon generation potential, and that of residual organic matter is close to exhaustion. Extracted samples exhibited the same trend of TOC values as pyrolysis samples. However, the TOC values of the extracted samples were all smaller than those of pyrolysis samples at different simulation temperatures, and the difference between the two represented the contribution of soluble organic matter (SOM) to the TOC content. It is noteworthy that the maximum difference between the two values is 1.42% at the simulated temperature of 350 °C, which implies that residual bitumen contributes the most to the TOC at the peak oil yield, about 32.5%.

The bitumen "A" content reaches a maximum value at the simulated temperature of 350 °C. As the residual bitumen continuously cracks into small molecule hydrocarbons and expelled, it decreases and approaches 0 at 500 °C. S_1/TOC value also increases and then decreases with the simulated temperature, but its peak temperature is relatively later compared to bitumen "A", which is caused by the fact that the generated free hydrocarbons need to satisfy themselves with adsorption and pore space retention before

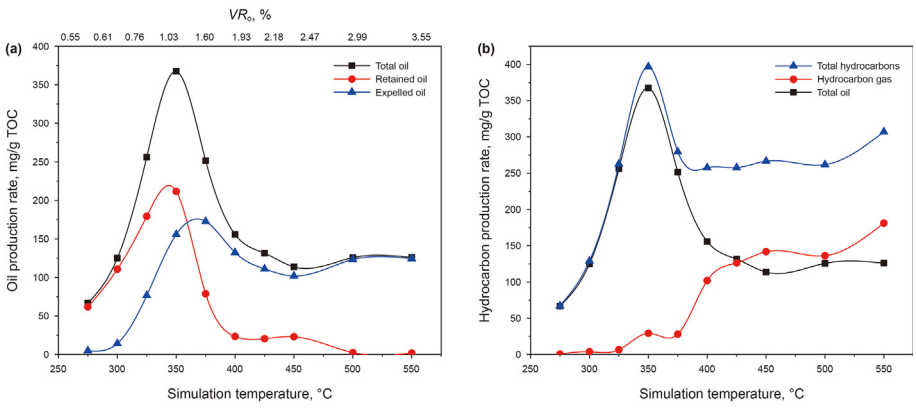

Fig. 5. Variation of generation-expulsion-retention hydrocarbon yields with increasing thermal evolution of organic-rich marl.

Table 4
Variation of organic geochemical parameters during hydrocarbon generation under near-geological conditions.

Sample ID.	Simulated temperature, °C	TOC_P, %	TOC_E, %	VR_o, %	S_1, mg/g	S_2, mg/g	HI, mg/g	T_{max}, °C	Chloroform bitumen "A", %
LQ-275	275	3.94	3.74	0.55	1.2	14.41	366	433	0.40
LQ-300	300	5.14	4.54	0.61	1.78	15.83	308	430	0.69
LQ-325	325	4.34	3.50	0.76	2.53	14.45	333	435	1.13
LQ-350	350	4.37	2.95	1.03	3.34	8.38	192	442	1.34
LQ-375	375	3.01	2.50	1.60	2.74	3.74	124	460	0.51
LQ-400	400	3.79	3.09	1.93	1.15	1.47	39	572	0.15
LQ-425	425	3.62	3.27	2.18	1.28	0.89	25	588	0.13
LQ-450	450	3.98	3.46	2.47	1.55	1.00	25	–	0.15
LQ-500	500	2.67	2.14	2.99	0.33	0.08	3	–	0.02
LQ-550	550	2.79	2.41	3.55	0.13	0.00	0	–	0.01

Note: TOC_P is the TOC value of the residue sample after pyrolysis experiment; TOC_E is the TOC value of a pyrolysis residue sample after the SOM has been extracted.

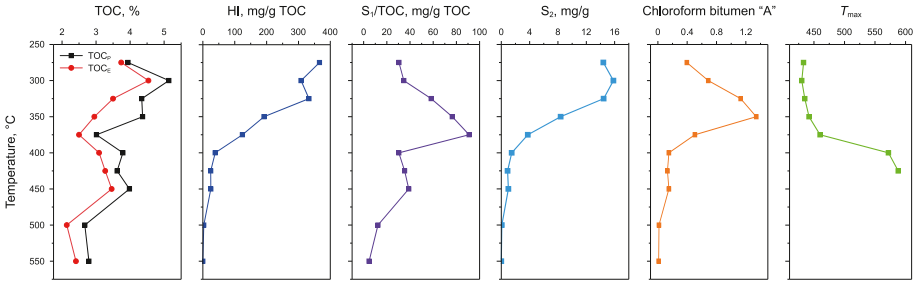

Fig. 6. Organic geochemical parameters evolution characteristics of pyrolysis samples.

they can be expelled in abundance. Particularly this value also has another small peak at the simulated temperature of 450 °C, which may be influenced by the inclusion OM and the hydrocarbon generation from organic acid salts (Xia et al., 2019; Wang et al., 2021). The S_2 value decreases continuously with increasing simulation temperature after 300 °C. The T_{max} value increases with increasing simulation temperature, especially rapidly increasing after 375 °C and up to 588 at 450 °C, which shows that the T_{max} value is not suitable for maturity judgment of pyrolyzed samples anymore.

3.3. Low-pressure gas adsorption test for rock pore analysis

3.3.1. CO_2 and N_2 adsorption curves

According to the IUPAC classification (Sing et al., 1985), the CO_2 adsorption isotherms of the original samples and simulated samples were of Type I, which exhibited monolayer adsorption (Fig. 7). The amount of gas adsorbed increases as the relative partial pressure within a relative pressure of 0.037. The nitrogen adsorption isotherms of 11 samples belong to Type IV (Sing et al., 1985) while developing a clear hysteresis loop (Fig. 8). When the relative pressure (P/P_0) is close to 1, as capillary condensation occurs, the amount of adsorption rises sharply and adsorption saturation is not reached. This reflects the presence of a certain amount of macropores in the sample. The hysteresis loops are dominated by H3 and H2 types, which indicates that the pores of the organics-rich marl samples are primarily of parallel-plate slit pores and ink-bottle pores. In addition, there are some other morphological pores.

The maximum CO_2 adsorption quantity was distributed between 0.44 and 1.44 cm^3/g (Fig. 9), with a maximum of 1.44 cm^3/g at the simulated temperature of 300 °C, which indicated that a great number of micropores were generated by the primary cracking of OM. It rapidly decreases to a minimum value of 0.44 cm^3/g near the peak of oil generation, meaning that the micropore PV is filled by retained oil and was not developed at this stage. Subsequently, it showed a wave-like increasing trend, with an adsorption quantity of 1.01 cm^3/g at 550 °C.

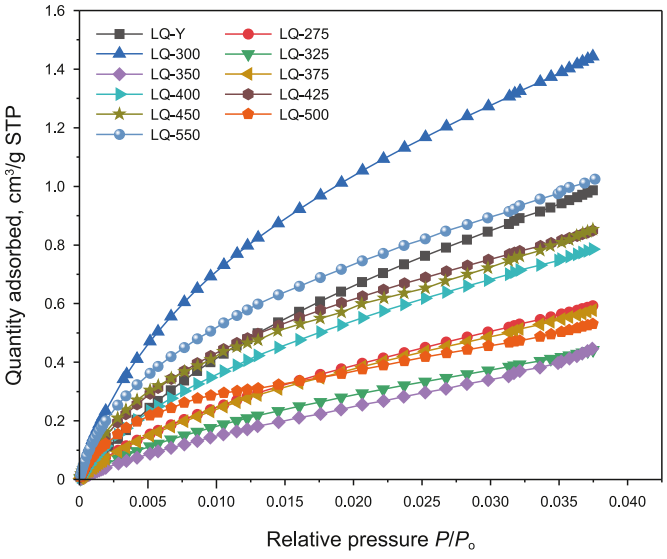

Fig. 7. CO_2 adsorption isotherm characteristics of original and simulated samples.

The trend of maximum N_2 adsorption with simulation temperature is like CO_2, with the difference that the rate of increase of N_2 adsorption is larger than that of CO_2 adsorption in the simulation temperature range of 325°C–450 °C, which implies that the rapid generation and development of macropore volume in this stage. During the simulated temperature range of 400°C–450 °C, the N_2 adsorption reached the maximum value of about 15.5 cm^3/g (Fig. 9).

3.3.2. Characterization of pore structure parameters

The pore structure parameters of micropores, mesopores as well as some macropores of the simulated and original samples were tested and analyzed by N_2 adsorption and CO_2 adsorption experiments, in which results are shown in Table 5. Micropores volume

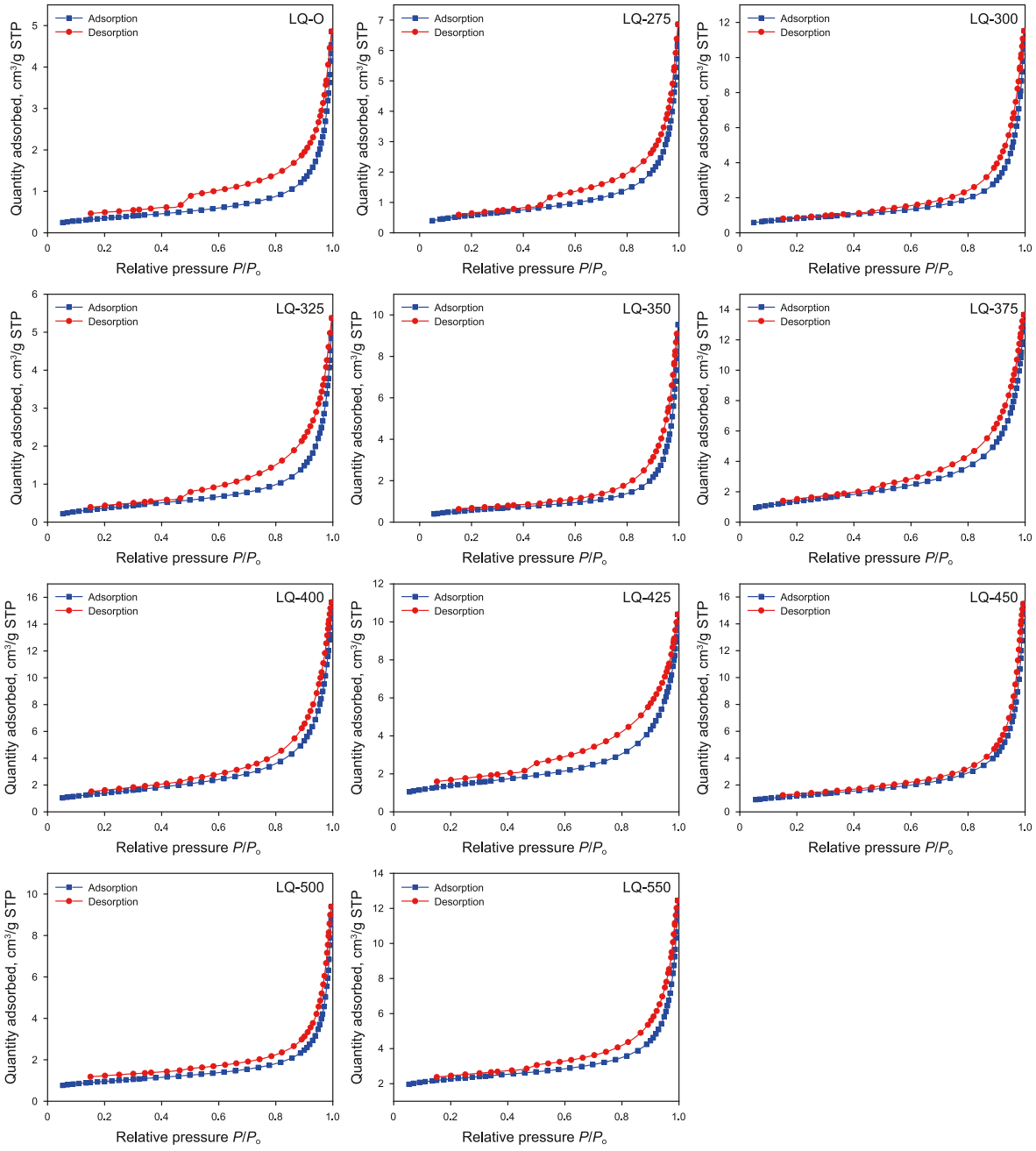

Fig. 8. Characteristics of nitrogen adsorption isotherms for raw and simulated samples.

were distributed between 0.233 and 1.528 cm^3/kg, while mesopores and macropores volume were distributed between 2.639 and 11.132 cm^3/kg and 3.903 to 12.073 cm^3/kg, respectively. Throughout the hydrocarbon generation process, the PV of micropores varied little and was much lower than that of mesopores and macropores. Both mesopores' and macropores' PV minimums occurred at earlier simulated temperatures than those of micropores, implying that SOM is preferentially retained in the pore slits dominated by mesopores and macropores, followed by micropores. Notably, the total PV and the BET Specific Surface Area of the simulated samples are larger than those of the original sample, which suggests that the hydrocarbon generation by OM would lead to an increase in the reservoir space, which agrees with (Jarvie, 2012).

3.3.3. *Pore size distribution*

The PSD curves for the micropores of the original and pyrolysis samples are shown in Fig. 10(a) and (b). The dV/dlog (W) has three distinct peaks at pore diameters of 0.45–0.65, 0.63 and 0.82 nm, indicating that the PV is more developed at the corresponding pore diameters, and the height of the peaks is obviously affected by the thermal maturity. Overall, except for the simulation temperature of 300 °C, the peak dV/dlog (W) of the pyrolysis samples before the simulation temperature of 400 °C is significantly lower than that of the pyrolysis samples after 400 °C. This implies that the gas window pyrolysis samples are more favorable for nanoscale pore development.

The PSD curves of mesopores and some macropores of the original and pyrolysis samples are shown in Fig. 10(c) and (d). With

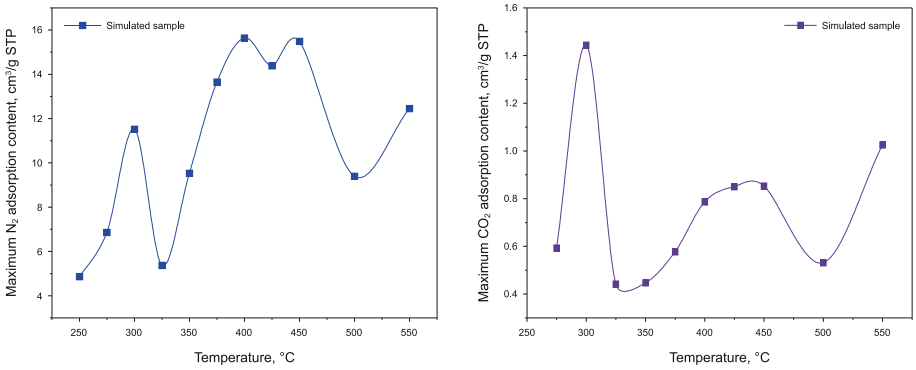

Fig. 9. Plot of maximum adsorption of nitrogen and carbon dioxide in pyrolysis samples at different simulation temperatures.

Table 5
Pore structure parameters of the original sample and pyrolyzed samples at different simulated temperatures.

Sample ID	Simulated temperature, °C	BET Specific surface area, m^2/g	Pore volume, cm^3/kg				Specific surface area, m^2/g			
			Micro pore	Mesopore	Macropore	Total pore	Micropore	Mesopore	Macropore	Total pore
LQ-O-	–	1.2892	0.798	2.639	3.903	7.340	2.432	0.878	0.125	3.436
LQ-275	275	2.1084	0.486	3.808	5.235	9.529	1.545	1.354	0.166	3.065
LQ-300	300	2.9208	1.528	6.478	9.130	17.136	1.589	2.040	0.301	3.930
LQ-325	325	1.4541	0.358	3.058	4.166	7.582	1.201	1.010	0.063	2.275
LQ-350	350	2.1216	0.233	5.015	8.128	13.376	0.740	1.490	0.263	2.493
LQ-375	375	5.0812	0.552	9.094	8.180	17.826	1.830	3.417	0.121	5.367
LQ-400	400	5.0457	0.810	10.091	10.209	21.110	2.533	3.520	0.347	6.399
LQ-425	425	3.9802	0.770	11.132	8.803	20.706	2.434	3.412	0.342	6.189
LQ-450	450	4.2169	0.901	8.629	12.073	21.603	3.031	2.833	0.432	6.297
LQ-500	500	3.2992	0.603	4.345	7.965	12.912	2.101	1.400	0.265	3.766
LQ-550	550	7.4571	1.124	5.993	8.741	15.859	3.714	1.994	0.288	5.996

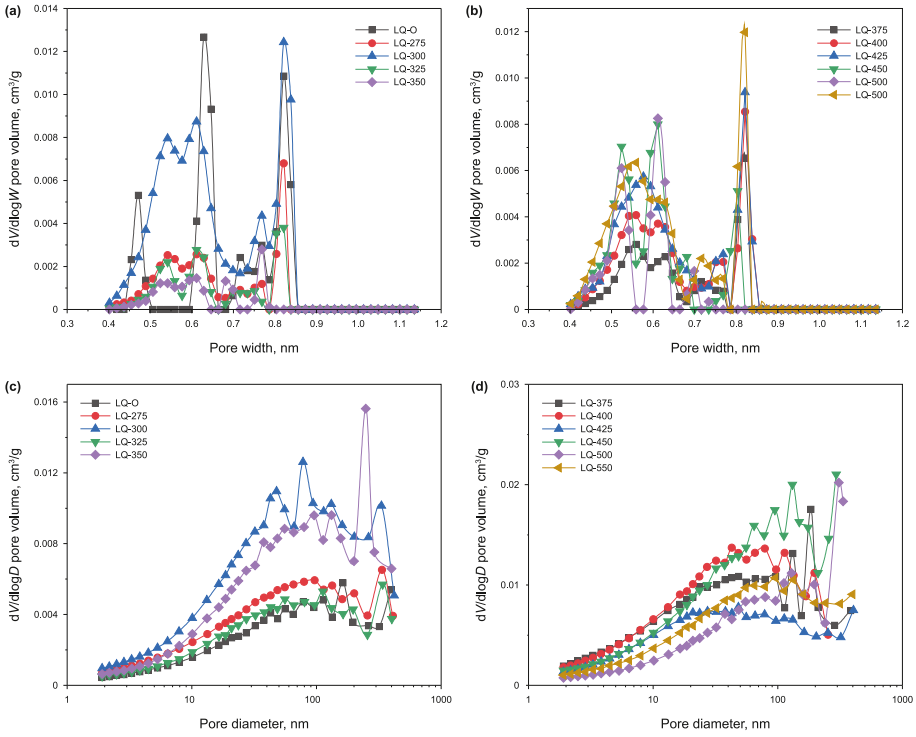

Fig. 10. PSD of the original sample and pyrolysis samples at different simulated temperatures. (**a**) and (**b**) are micropores; (**c**) and (**d**) are mesopores and some macropores.

the increase of pore size, d*V*/dlog (*W*) also increases gradually, especially the d*V*/dlog (*W*) of pores larger than 10 nm is obviously larger than that of smaller pores. It indicates that the pores larger than 10 nm provide more reservoir space for hydrocarbons. The d*V*/

dlog (W) curves of the pyrolysis samples at simulated temperatures of 400 and 450 °C are significantly higher than those of the other pyrolysis samples, indicating that the mesopore and macropore volumes of the samples are more developed at this evolutionary stage. A simulation temperature of 500 and 550 °C pyrolysis samples dV/dlog (W) curves are significantly lower than those of the samples in the temperature range of 375 to 450 °C, implying a decrease of PV.

3.4. Based on FE-SEM pore morphology characterization

Based on the OM genesis, type and thermal maturity, OM can be categorized into primary kerogen OM and secondary migration OM (bitumen), both of which are important carriers of OM pores development (Loucks and Reed, 2014). It is easy to distinguish between kerogen and bitumen in terms of distribution morphology and size. The former generally has a relatively fixed shape and structure, showing clumps and strips distributed in the matrix minerals. While the latter is formed by the migration of liquid hydrocarbons into the mineral matrix pores, generally with irregular morphology, which further evolves into solid bitumen and pyrobitumen at highly evolved stages with the development of OM pores (Bernard et al., 2012; Liu et al., 2022a; Zhang et al., 2022). According to the classification of pore types by Loucks et al. (2012) and Yang et al. (2019), mineral matrix pores such as calcite residual intergranular pores, grain edge seams and intragranular dissolution pores are predominant in the original samples (Fig. 11). Very few OM pores can be observed in kerogen, which may be related to the type of kerogen and biochemical gas generation (Ma et al., 2017). Some migrated OM can be seen to have filled between the pores of the mineral matrix that blocked the intergranular pores. This shows that the original sample has undergone the process of hydrocarbon generation and is in the low maturity stage. In addition, some OM can be observed to combine with clay minerals to form an organic-clay complex, with no obvious pore development within.

OM pore development of pyrolyzed samples is clearly controlled by thermal maturity and hydrocarbon generation-expulsion-retention process. It mainly develops kerogen OM pores, bitumen pores, organic-clay complex pores and OM shrinkage cracks. Meanwhile, mineral matrix pores such as intergranular pores, intercrystallite pores, intragranular dissolution pores and grain edge seams are also developed to different degrees.

4. Discussion

4.1. Pore structure evolution during hydrocarbon generation

4.1.1. Pore volume and specific surface area evolution characteristics

The values of PV and SSA are key parameters for the evaluation of unconventional oil and gas resources in organic-rich marl (Chen et al., 2018; Wang and Guo, 2021; Cao et al., 2022). Statistical analysis of the pore structure parameters of pyrolysis samples shows that mesopores and macropores are similar in the PV evolution trend, both of which are primary contributors to the PV of the samples at different evolutionary stages (Fig. 12(a) and (c)). Compared to lacustrine and marine shales, macropores are more developed in organic-rich marl (Xu et al., 2021; Wang et al., 2023c). After the peak oil yield stage (T = 350 °C), the SSA contribution of micropores showed an increasing trend, especially after the overmature stage (T = 450 °C), where the SSA of micropores gradually dominated (Fig. 12(b) and, (d)). More than 90 % of the total SSA is contributed by micropores and mesopores, which together provide more adsorption sites for hydrocarbon gases. Based on the evolution law of PV and SSA of the simulated samples, we can roughly classify the pore structure evolution characteristics of organic-rich marl into four stages during the hydrocarbon generation evolution.

The first stage is a rapid increase in PV (275 °C < T ≤ 300 °C), in which the OM is first cracked to form lots of mesopores and macropores, with rapid increase of PV. A lot of generated oil can't be discharged and is retained in the reservoir. The second stage is a rapid decrease in PV (300 °C < T ≤ 325 °C), which corresponds to the stage of mass bitumen generation, and the bitumen fills up the mineral matrix pores and OM pores, resulting in a rapid decrease of the PV, as well as the SSA (Zhang et al., 2022). also confirmed the “pore-reducing effect” that residual oil filling the pores of calcareous shale at the early stage of maturity.

The third stage is a rapid increase in PV (325 °C < T ≤ 450 °C), which corresponds to the late maturity stage and the high maturity stage. The kerogen thermal degradation gas and retained oil cracking gas led to a rapid increase in gas yield (Fig. 5), while forming many OM pores. Especially within the simulated

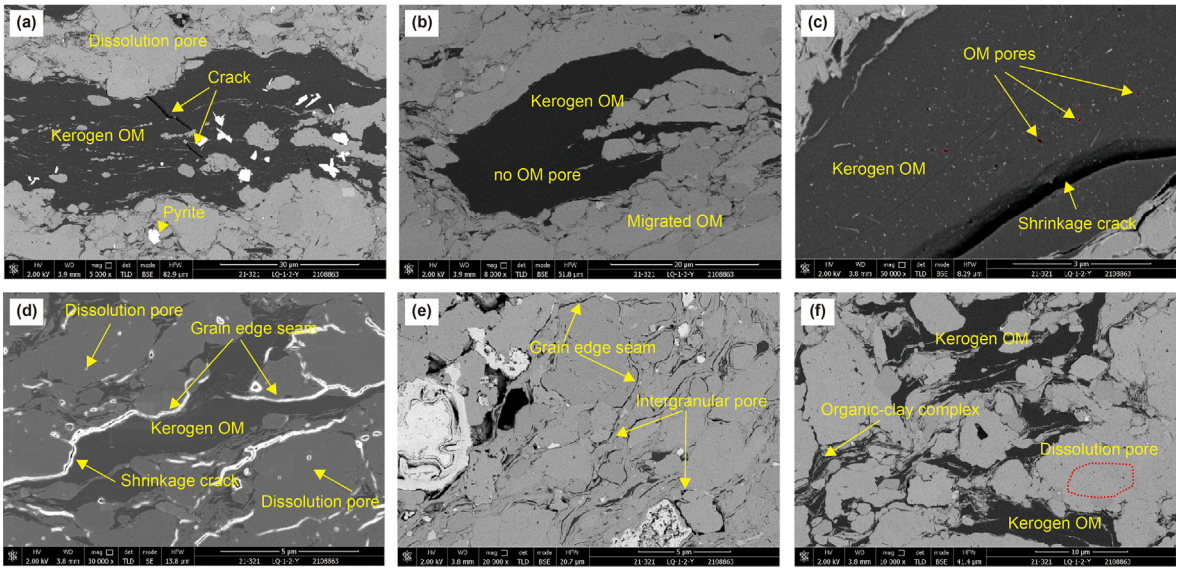

Fig. 11. Pore development characteristics of the original sample from organic-rich marl under FE-SEM.

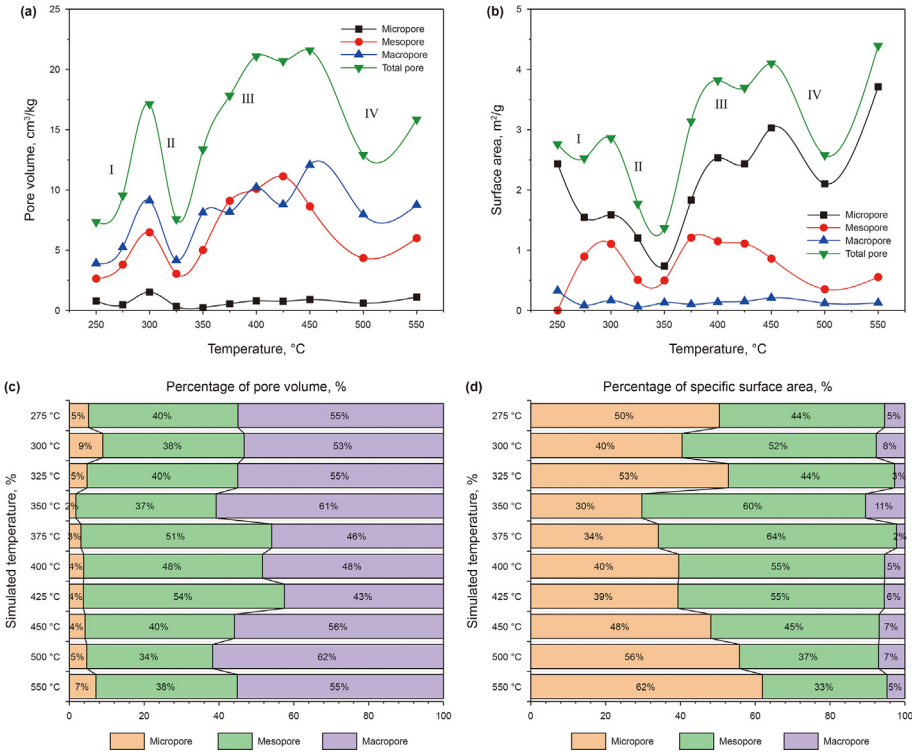

Fig. 12. Characteristics of PV, SSA evolution as well as percentage of the whole process of hydrocarbon generation in organic-rich marl. **(a)** and **(b)** are PV; **(c)** and **(d)** are SSA.

temperature range of 400–450 °C, which is the peak period of retained oil cracking gas, and the peak interval of PV and SSA development, conducive to the exploration of unconventional natural gas. The fourth stage is a rapid decrease in PV followed by stable development (450 °C < $T \leq$ 550 °C), which corresponds to the overmature stage with increasing lithostatic pressure (Table 3) and more efficient oil drainage. The formation pore pressure is unable to resist the strong compaction, resulting in OM pores collapse and a rapid decrease in total PV, as well as in total SSA.

Moreover, we further analyzed the correlation between hydrocarbon yield and total PV. The results indicated that the retained oil yield showed a negative linear correlation with the total PV, $R^2 = 0.55$ (Fig. 13(a)), but the hydrocarbon gas yield showed a positive linear correlation with total PV, $R^2 = 0.56$ (Fig. 13(b)). This implies that at the low mature-mature stage ($VR_o < 1.03$) retained oil content is higher, so that PV decreases to a certain extent. The hydrocarbon gas yield at this stage is relatively low, and the main source is the thermal degradation of kerogen. With the increase of thermal evolutions, a large amount of retained liquid hydrocarbons are cracked into gas at the high over-mature stage ($1.6\% \leq VR_o \leq 3.55\%$), meanwhile generating numerous nanoscale OM pores. The results exhibit that retained oil content decreases rapidly, and the PV increases further. In summary, a high retained oil rate at the peak of oil generation provides an abundant material basis for gas formation at high maturity and over maturity stage. Combined gas supply from early thermal degradation of kerogen and late retained hydrocarbon cracking ensures that the organic-rich marl still has excellent gas exploration potential in the high maturity and over maturity stage (Fig. 5).

4.1.2. Hydrocarbon generation and organic matter pore formation

The development of OM pores is closely related to OM abundance, type, thermal maturity (R_o) and hydrocarbon generation (Kuang et al., 2022; Milliken et al., 2013). In fact, OM pores formation and preservation is a dynamic process influenced by R_o and diagenesis (Guo et al., 2020; Liu et al., 2022b). FE-SEM observations

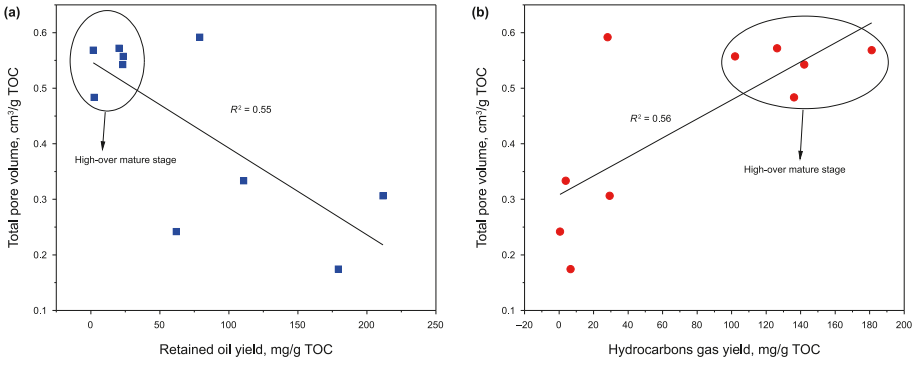

Fig. 13. Correlation between hydrocarbon yield and total PV evolution in organic-rich marl.

show that the OM pores of the organic-rich marl samples obtained from pyrolysis experiments with different VR_o are primarily composed of kerogen OM pores, bitumen pores and OM shrinkage cracks.

Formation and evolution of kerogen OM pores and bitumen pores are mainly controlled by hydrocarbon generation of OM and diagenesis. When the simulated temperature ≤350 °C, kerogen is dominated by the generation of liquid hydrocarbon and forms a small number of oval and circular OM pores at its interior, while overall OM pores development is not obvious (Fig. 14(a)–(d)). It may be attributed to the low oil expulsion at this stage, where the generated liquid hydrocarbons are mainly stored as retained oil within the kerogen, partially migrated into the intergranular pores or adsorbed on the mineral surfaces. Due to the filling effect of massive bitumen on the OM pores, it impeded internal pore development in the OMs. Löhr et al. (2015) used Soxhlet extraction to remove bitumen from mature shale that previously had not developed OM pores, unsurprisingly, the extracted samples showed a significant amount of OM pores under FE-SEM, which further supports the above view. Similarly, the TOC values of the extracted samples from the main oil generation stage were much smaller than those of the pyrolysis samples, which may be a further indication that the OM pores are easily occupied by bitumen. Therefore, at $R_o \leq 0.76\%$ low maturity and early maturity stages, the OM pores within the kerogen are not developed.

Furthermore, the formation and evolution of OM pores in kerogen are heterogeneous. When the $VR_o = 0.55\%$, the development of OM pores was visible in the early maturity stage with pyrite participation in the OMs (Fig. 14(b)), which possibility was related to the interaction between OMs and pyrites (Ma et al., 2016). When the $VR_o = 1.93\%$, FE-SEM observation showed that one type of kerogen internal OM pores were densely developed with PSD range from 20 nm to 300 nm, while the other type of kerogen OM was basically undeveloped pores and only very few OM pores existed (Fig. 14(g) and (h)). Curtis et al. (2012) observed a similar phenomenon in the geological samples of the Woodfood Shale at $VR_o = 1.4\%$. Although the same samples have experienced the same thermal evolution, OM pore development varies considerably. We infer that R_o is not the only controlling factor for the development of OM pores, while the type of OM and the participation of

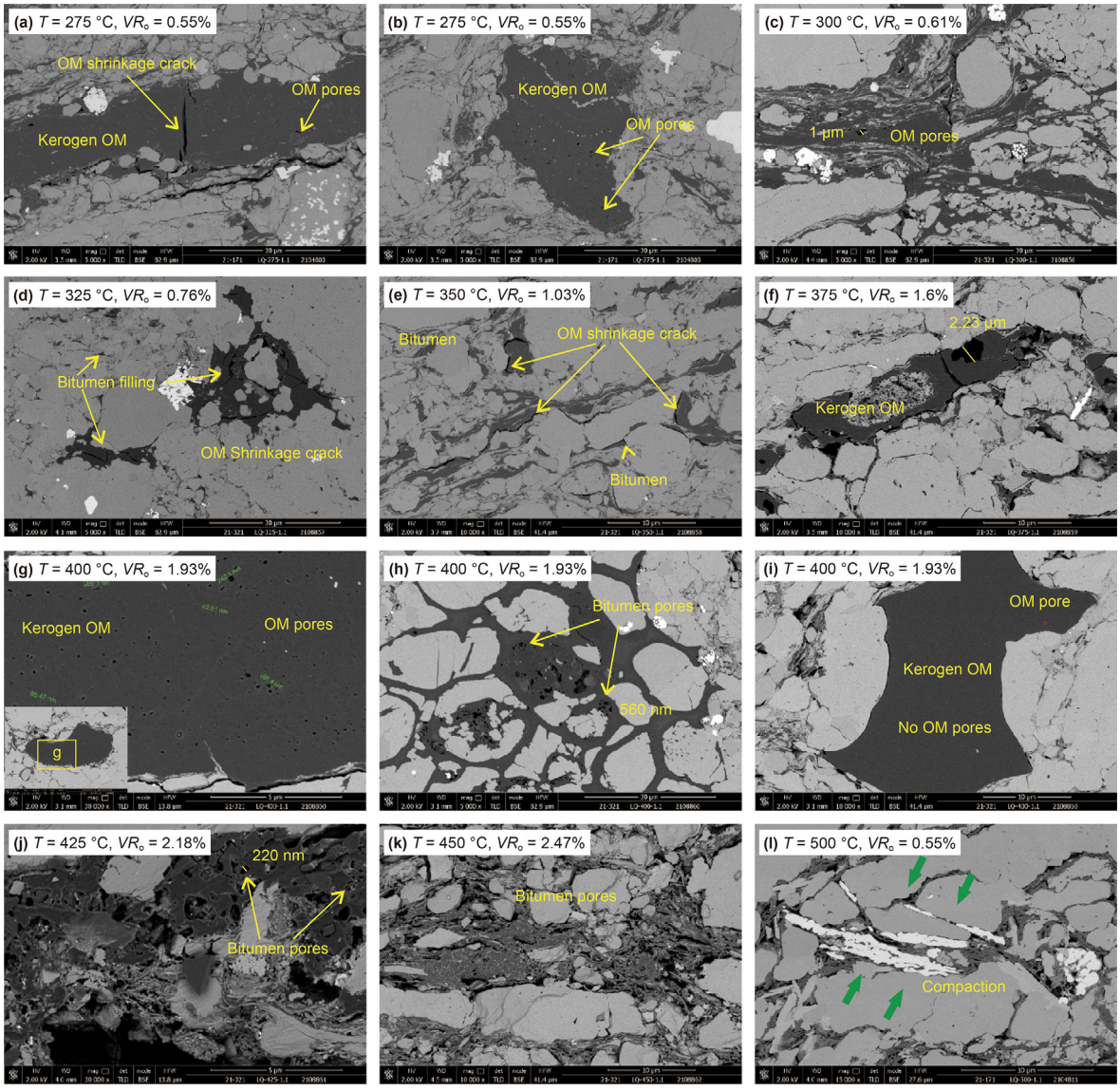

Fig. 14. OM pore development characteristics during hydrocarbon generation-expulsion-retention processes.

inorganic minerals also play an important role in the formation and development of OM pores.

With the degree of thermal evolution increasing further, oil expulsion was enhanced and OM pore development became more pronounced (Figs. 5 and 14). Generally, the PSD of OM pores produced by oil generation is large and can reach the micrometer scale (Fig. 14(c) and (f)). When the degree of thermal evolution increases to the late maturity stage and the high maturity stage, which is the stage of thermal cracking to generate gas ($1.03\% < VR_o < 2.47\%$), migration OM begins to heavily crack to generate hydrocarbon gas, resulting in many nanoscale pores (Fig. 14(h)–(k)). Especially after $VR_o \geq 1.6\%$, the internal pores of the bitumen began to develop in large quantities, showing circular, oval and irregular shapes, with the total PV value being approximately twice as much as that of the original samples (Table 5, Fig. 14(h)). At the high maturity and over maturity stages, pores are generally densely distributed over large areas, with a spongy, honeycomb-like morphology dominating (Fig. 14(g)–(j)). VR_o at 1.93%–2.47% was the peak of hydrocarbon gas generation by thermal cracking, and the peak interval of bitumen pore development (Fig. 5; Fig. 12), where adjacent small pores could be further enlarged and merged into large pores, which further improved the connectivity of the OM pores and increased the adsorption of hydrocarbon gases. At $VR_o > 2.47\%$, because a large quantity of retained bitumen cracked to generate hydrocarbon gas as well as discharged out of the hydrocarbon source rock, which resulted in a reduction of formation pore pressure, the previously formed circular and oval OM pores will be further narrowed, deformed and even disappeared.

OM shrinkage cracks are mainly related to the volume decrease of OM during hydrocarbon generation, which are presented in samples of different thermal maturity, and most frequently in the stage of oil generation. They are mainly distributed in the internal and edge of OM (Fig. 14(a)–(e) and (f)) that perform a critical role in hydrocarbon migration and accumulation.

4.1.3. Pore formation and development controlled by organic-inorganic interactions

The interaction between OM and inorganic mineral components is a critical mechanism in the hydrocarbon generation and reservoir process of organic-rich shales. It mainly includes the interaction of OM with clay minerals, OM with pyrite and OM with unstable minerals such as calcite and feldspar (Cai et al., 2023; Ma et al., 2016, 2022; Zhu et al., 2020). In fact, in addition to the kerogen and migrated bitumen discussed above, part of OM in organic-mineral complexes exist while developing organic pores during hydrocarbon formation and evolution of organic-rich marl. The common organic-mineral complexes in this study are mainly organic-clay complexes and organic-pyrite complexes.

Through FE-SEM observation and analysis of the samples with different maturity obtained by pyrolysis, it was found that the organic-clay complexes mainly have two types of microscopic distribution forms. One is that due to the strong adsorption of clay minerals during sedimentation and diagenesis, thus promoting the preservation of some algae in the form of organic-clay complex. FE-SEM shows that the clay minerals are seen to be tightly bound to the organic matter, and the direction of extension is consistent with the direction of the laminae, which are highly oriented. This type of organic-clay complexes is controlled by oil expulsion mechanisms during the main oil generation stage usually generates shrinkage cracks in the OM interior and margins, as well as the formation of large internal OM pores (Fig. 15(a), (b), (e)).

The other is that during hydrocarbon generation, partial liquid hydrocarbons are migrated and filled into the inorganic mineral pores associated with the interlayer pores of clay minerals, which adhere to the surfaces and interlayers of clay minerals by physical adsorption. Clay minerals with gray flakes and dark OM can be clearly distinguished under the FE-SEM, and traces of bitumen fills are clearly visible (Fig. 15(c), (d), (h), (i)). The process of generating micro and nanoscale pore seams in this type of organo-clay complexes is like the mechanism of bitumen pore development discussed above. However, the difference is that because of the catalytic pyrolysis of clay minerals, the bitumen in the organo-clay complex has a higher degree of thermal degradation and more pores are easily exposed (Wang et al., 2023b). collected petrophysical and geochemical data for numerous samples of marl from the Leikoupo formation, which indicate that there is a strong positive correlation between clay mineral content with both TOC and porosity values, the organic-clay complex pores may have a critical role in contributing to the porosity. On the one hand, the strong adsorption of OM by clay minerals is conducive to enhancing the hydrocarbon potential of the marl itself. On the other hand, the organic-clay complex cracks to form many micro-nano pore seams during the high evolution stage, which can significantly increase the reservoir space and provide an effective channel for hydrocarbon accumulation and flow.

Besides the organic-clay complex pores, OM is often associated with pyrite and fills the intercrystallite pores of pyrite while developing OM pores (Fig. 14(l); Fig. 15(e) and (f)). It is usually that the liquid hydrocarbons generated in the low maturity-maturity stage are filled with pyrite intergranular grains and further cracked into gas in the high maturity stage, which provides favorable support for the preservation of the OM pores due to the high resistance to compaction of the pyrite grains. Moreover, the catalytic effect of hydrocarbon generation by pyrite may further promote the formation of OM pores (Li et al., 2022). Overall, the pores of the organics-pyrite complex are mostly circular and oval, with PSD between 30 and 220 nm and better connectivity.

With the increase of thermal evolution, the thermal degradation of kerogen to generate oil was accompanied by the generation of abundant gases (CH_4, CO_2, H_2S, etc.) and a number of organic acids (Cao et al., 2021; Xu et al., 2021). The acidic fluids can induce the dissolution of unstable minerals to form irregularly shaped secondary dissolution pores within or at the edges of the grains, which promotes the development of reservoir, while part of the pores is filled with bitumen (Fig. 16(a) and (b)). Calcite is the most abundant in the samples of this study, which is more intensely dissolved by organic acids, so calcite dissolution pores are most likely to develop. At the simulated temperature of 325 °C, calcite dissolution pores are not obvious, with the enhanced hydrocarbon generation, calcite dissolution pores begin to develop abundantly, which can constitute a complex pore-seam-network reservoir with mineral matrix pores such as grain edge seams and intergranular pores in the high evolutionary stage (Fig. 16(c), (d), (e)). On one hand, the interaction between organic acidic fluids and inorganic minerals in the maturity stage forms a great number of secondary dissolution pores, which effectively improve the reservoir space. On the other hand, the bitumen generated by the thermal degradation of kerogen at the low thermal evolution stage was filled in the dissolution pores, and further cracked to form natural gas and solid bitumen at the high evolution stage while developing OM pores in its interior, which further provides effective reservoir for hydrocarbon enrichment.

4.1.4. Diagenesis and inorganic mineral pore formation

By analyzing the FE-SEM, SEM and EDS image characteristics of solid cylinder samples with different maturity levels, combined with low-pressure gas adsorption pore parameters, the results indicate that compaction, clay mineral transformation, as well as cementation and recrystallization filling are the main diagenetic effects modes. The compaction has a significant pores reduction

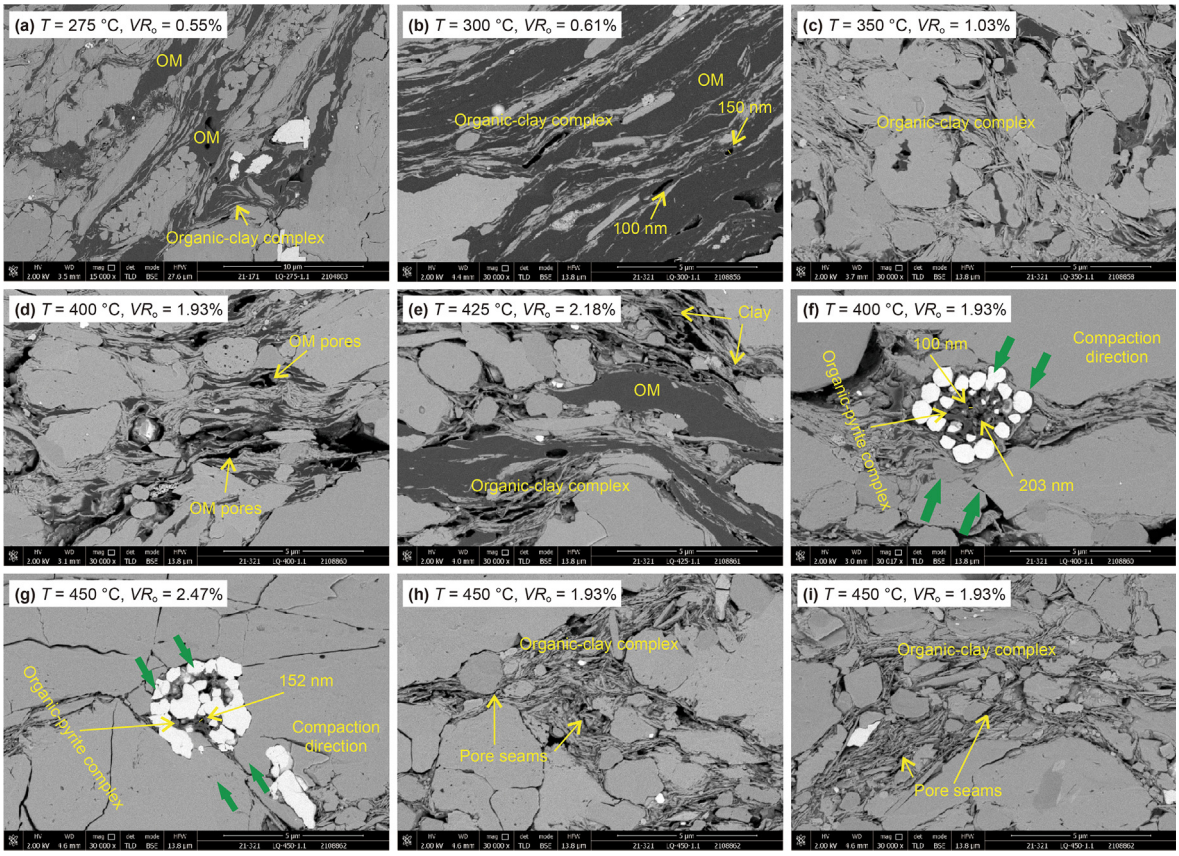

Fig. 15. Pore development characteristics of organic-mineral complexes during thermal evolution.

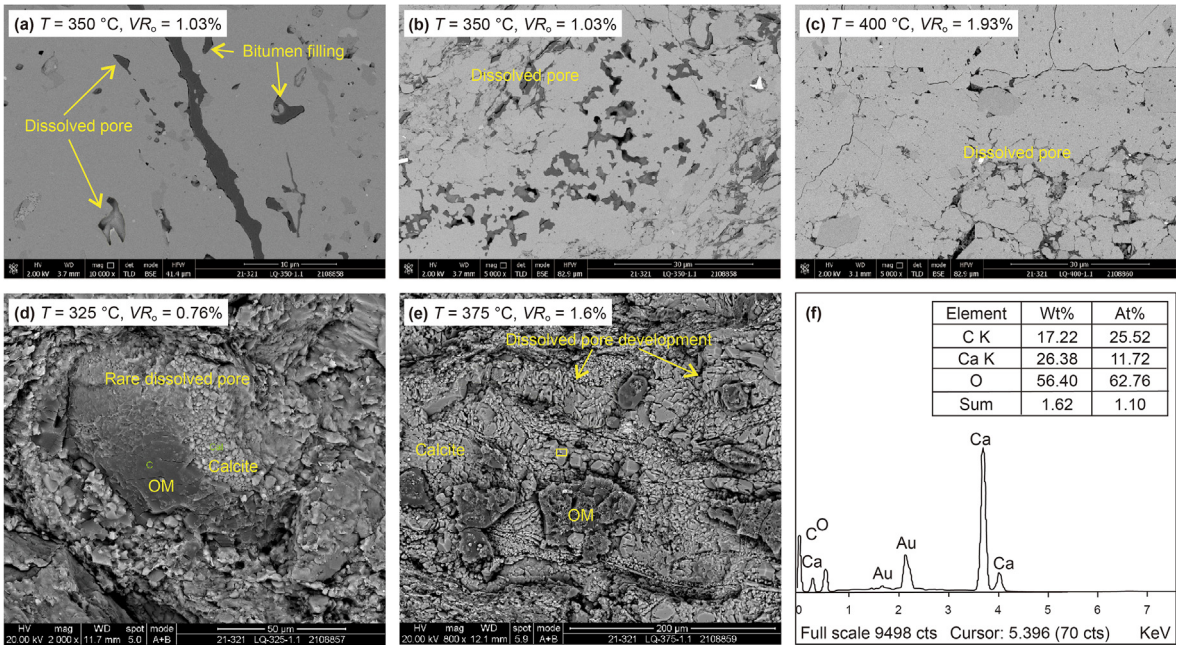

Fig. 16. Pore development characteristics of acidic fluids interacting with carbonate minerals. **(f)** Is the energy spectrum of **(e)**.

effect in the early diagenetic stage (Loucks et al., 2012; Mastalerz et al., 2013), where residual intergranular pores and grain edge seams that are unfilled by bitumen are the predominant type (Fig. 17(a)). Due to the decrease of formation pore pressure in the late over-mature stage, compaction has a destructive effect on the previously formed OM pores. In the middle diagenetic stage, clay minerals adsorbed a great quantity of migrated bitumen to fill in the interlayer pores, which forms an organic-clay complex (Figs. 15

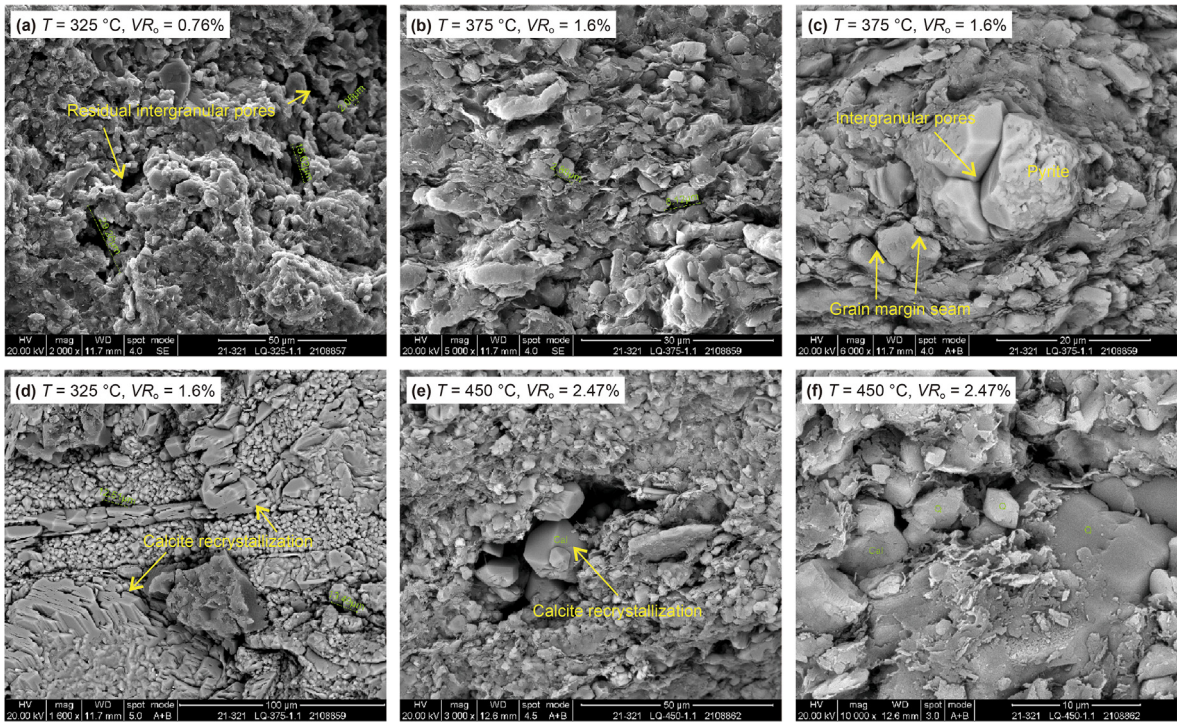

Fig. 17. Characteristics of major diagenesis and inorganic mineral pore development during thermal evolution of organic matter.

and 17(b)). Simultaneously, during clay mineral transformation, Ca^{2+} and Mg^{2+} were released to break the original water-rock equilibrium, resulting in calcite recrystallization and quartz secondary enlargement, which occupied the pore space and seepage channels (Figs. 15(h) and 17(d) and (e)). Grain-edge seams are mainly distributed at the edges of carbonate or quartz minerals and play an important role in connectivity for hydrocarbon migration (Fig. 17(b), (c), (f)). The natural gas in high maturity and overmaturity stages will also diffuse into the grain-edge seams after satisfying its own OM pores adsorption enrichment, which is supported by the exploration of marl samples from one section of the Maokou Formation in the Sichuan Basin (Su et al., 2021). Furthermore, pyrite intergranular pores can be better preserved at high evolutionary stages due to the strong anti-compaction ability of pyrite crystals (Fig. 17(c)).

4.2. Pore evolution model and exploration implications

4.2.1. Contrast with other shale pore volume evolution

Previous research has focused on the pore evolution characteristics of marine and lacustrine organic-rich shales utilizing the same semi-enclosed hydrous pyrolysis experiments, which provides ideal data for better comparison the differences between the pore evolution of marine organic-rich marls and other shales. The data used to compare the marine siliceous shale were obtained from (Cao et al., 2021). The TOC and VR_o values were 9.83% and 0.63%, respectively. Mineral compositions are dominated by quartz (56.5%), calcite (25.9%), and clay minerals (10.4%), along with small amounts of feldspar and pyrite. Data used to compare the lacustrine shales were obtained from (Song et al., 2022), with TOC and VR_o values of 17.49% and 0.88%, respectively. The kerogen type of all samples was Type II_1, which is consistent with the marl samples in this study. From Fig. 18(a), the trend of PV evolution of marine silicic shale is like that of marl before the overmature stage ($VR_o \approx 2.5\%$, $T = 450\ ^\circ C$), and the retention reservoir space of marl is larger than that of silicic shale. This indicates that the oil retention capacity of marine organic-rich marl is better than that of marine shale, with a large amount of oil retained in the intra-source reservoir space, which is conducive to cracking into gas at a higher evolutionary stage. The results are in accordance with the pyrolysis experiments of (Huang et al., 2023). Notably, there is little difference in PV between the two from the early maturity stage to the peak oil generation stage. However, the PV of marine organic-rich marl is much larger than that of siliceous shale in the late to high maturity stage ($1.0\% < VR_o < 2.5\%$). There are two main reasons attributed to this. One is that compared to organic-rich shale, marl has a higher calcite content, which is more likely to react with acidic fluids such as organic acids and CO_2 in a water-rock reaction, and the pore-increasing effect of organic-inorganic interactions is obvious. Another is that the carbonate mineral framework plays a critical role in OM pore preservation, which is the "anti-pressure and pore preservation". A peak of PV development in the marine shale after the overmature stage is related to its high TOC content, which is the result of the coupled evolution of hydrocarbon generation and diagenesis (Xu et al., 2021). PV values of the lacustrine shale are lower than those of the marine marl during the entire evolutionary stage, even though the former has a higher TOC value (Fig. 18(b)). It is mainly attributed to the development of the laminated structure of lacustrine shales with high oil expulsion efficiency and the lack of a rigid mineral framework to resist the compaction of the overlying formation pressure (Borjigin et al., 2021; Huang et al., 2023). Moreover, the low contribution of OM pores in lacustrine shales compared to marine shales is another reason (Song et al., 2020b).

4.2.2. Pore evolution model for marl

Combined with the pore morphology and structure evolution law during hydrocarbon generation evolution, this paper divides the pore evolution of marine organic-rich marl into four stages with R_o as the main division index, as well as establishes an evolution model diagram (Fig. 19).

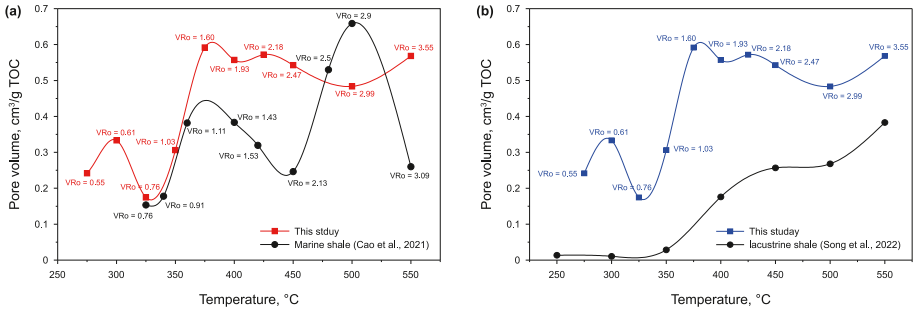

Fig. 18. PV evolution of organic-rich marl characterized by comparison with other shales.

In the low maturity to early maturity stage ($0.5\% < VR_o \leq 0.76\%$), with the increase of thermal evolution, the kerogen OM began to degrade to generate liquid hydrocarbons and some associated gases. The primary cracking effect of kerogen forms OM pores and shrinkage cracks both inside and edge of the OM, while the PV and SSA all show increase slightly. Part of the hydrocarbons not expelled from the source rock system are adsorbed inside the kerogen, and part of them are filled in the mineral intergranular pores and intragranular pores, coupled with the continuous compaction, the PV reaches the minimum value when VR_o is 0.76%. At this stage, the OM pores are undeveloped, mainly dominated by inorganic mineral matrix pores, OM shrinkage cracks and grain-edge seams.

In the mature stage ($0.76\% < VR_o < 1.6\%$), the extent of kerogen cracking increased, while the bitumen previously filled in the intergranular and intragranular pores of minerals began to crack into wet gas, and the quantity of organic pores began to increase, but the inorganic mineral matrix pores were still dominant. The supporting effect of retained hydrocarbons and high pore fluid pressure at this stage is favorable to the preservation of pores. In addition, the dissolution of carbonate minerals by acidic fluids derived from the hydrocarbon generation of OM also increases the reservoir space to a certain extent.

In the high-maturity to over-maturity stage ($1.6 \leq VR_o \leq 3.0\%$), As VR_o increases to 1.6%, the kerogen is heavily degraded to gas, the extent of bitumen cracking increases, and both kerogen OM pores and bitumen OM pores are beginning to develop in large quantities, which maturity is the lower limit for the development of abundant OM pores in marine organic-rich marl. When the VR_o is in the range of 1.9% to 2.5%, the kerogen is affected by the time and intensity of thermal evolution, the graphitization is intensified, gas generation potential is decreased, as well as the pores of the kerogen OM is gradually reduced. The bitumen and organic-clay complex succeeded the kerogen as the main hydrocarbon generation material as well as formed a great number of OM pores, which together with the intergranular pores and grain edge seams constitute a complex pore-seam-network system providing an important reservoir space for unconventional carbonate gas. When $VR_o > 2.5\%$, due to the reduced content of retained hydrocarbons, the formation pore fluid pressure is unable to support the strong compaction effect of the overlying formation pressure leading to PV decrease.

In the metamorphic stage ($VR_o > 3.0\%$), both kerogen, bitumen and organic-clay complex OM are strongly carbonized, aromatization enhanced, and the physicochemical properties tend to graphitization. The previously formed OM pores are further transformed from elliptical or circular to pinhole-like, which occurs closure, reduction or even disappears. At this stage, under the double impact of strong compaction and OM carbonization, the PV of the rock decreases dramatically, and the property of the reservoir undergoes a fundamental change.

4.2.3. *Implications for unconventional oil and gas exploration*

In recent years, unconventional natural gas exploration in the marine marl of the Permian-Triassic Maokou Formation and Leikoupo Formation has achieved significant discoveries in Sichuan Basin, South China (Su et al., 2021; Wang et al., 2023b). Considering

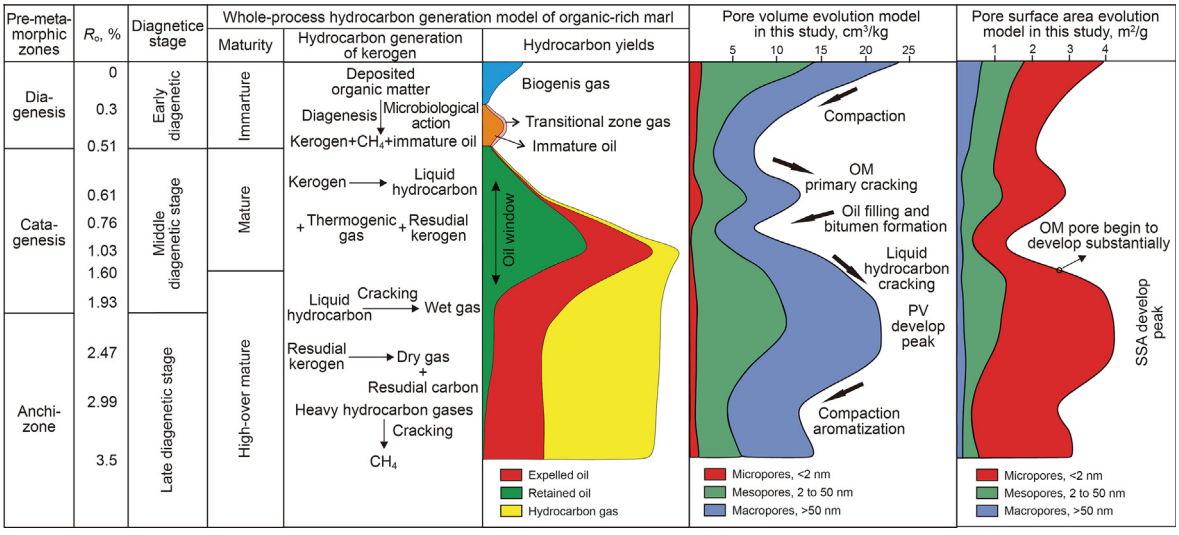

Fig. 19. Pore evolution model for the whole process of hydrocarbon generation in marine organic-rich marl.

that most of the marine marls in the Sichuan Basin are in the high mature-overmature stage, combined with the above discussion and pyrolysis experimental understanding, this study provides three insights to predict the dessert zones for this new type of unconventional oil and gas reservoirs. (1) The VR_o within the range of 1.9%–2.5% is favorable for the exploration and development of unconventional marl natural gas. (2) The overpressure condition and the coupling of rigid mineral framework are beneficial to the preservation of pores which provide effective reservoir space for hydrocarbon enrichment. (3) Organic-inorganic interactions not only enhance the hydrocarbon potential of the marl, but also improve the hydrocarbon reservoir space. The results of this study have significant guiding significance for the exploration of new layers, new fields and new types of marl in the Sichuan Basin of China, and can also provide ideas and references for unconventional natural gas exploration in other basins.

5. Conclusion

In this paper, by taking the marine low-mature organic-rich marl as the research object we analyzed the pore formation and evolution mechanism during the hydrocarbon generation-expulsion-retention process based on hydrous pyrolysis simulation experiments under near-geological conditions. The main insights obtained are as follows:

1. With increasing thermal evolution, the total oil yield and retained oil peaked at $VR_o = 1.03\%$, which were 367.51 mg/g TOC and 211.67 mg/g TOC, respectively. At the peak of oil generation, high retained oil yield provides an abundant material basis for gas formation by retained oil cracking in the high-over maturity stage. Combined gas supply from early thermal degradation of kerogen and late retained hydrocarbon cracking ensures that the organic-rich marl still has excellent gas exploration potential in the high maturity and over maturity stage.
2. Organic-rich marl pore formation and evolution are controlled synergistically by hydrocarbon generation, diagenesis, and organic-inorganic interactions, and the pore structure evolution process can be divided into four stages. Primary cracking of organic matter at the low maturity stage and secondary cracking at the high evolution stage increase the PV, and residual bitumen at the oil window stage will block the formed PV. Strong compaction and aromatization at the overmature stage would gradually decrease the PV.
3. The retained reservoir capacity of the marine organic matter-rich marl is greater than that of the marine shale and lacustrine shale. Organic acidic fluids in the maturity stage have obvious dissolution effects on carbonate minerals, lots of bitumen pores and organic-clay complex pores formed by hydrocarbon generation in the high maturity stage have remarkable pore growth effects, which together with the intergranular pores and grain-edge seams form a complex pore-seam-network system that provides a vital condition for unconventional gas accumulation and reservoirs.
4. The VR_o limit of OM pore mass development in marine organic-rich marl is about 1.6%. The PV and SSA are at their highest values within the maturity range of 1.9% to 2.5%, which is the optimal period for pore development and is conducive to exploring unconventional natural gas.

CRediT authorship contribution statement

Tong Wang: Writing – original draft, Methodology, Investigation, Conceptualization. **Xiao-Feng Wang:** Validation, Methodology. **Dong-Dong Zhang:** Visualization, Investigation. **Qing-Tao Wang:** Formal analysis, Data curation. **Hou-Yong Luo:** Resources, Methodology. **Jie Wang:** Visualization, Data curation. **Zhong-Liang Ma:** Resources, Conceptualization. **Zhang-Xing Chen:** Writing – review & editing, Supervision. **Wen-Hui Liu:** Writing – review & editing, Supervision, Funding acquisition.

Declaration of interests

The authors declare that they have no known competing financial interests or personal relationships that could have appeared to influence the work reported in this paper.

Acknowledgements

This research was supported by the National Natural Science Foundation of China (Grant No. 41930426).

References

Bernard, S., Horsfield, B., Schulz, H.M., et al., 2012. Geochemical evolution of organic-rich shales with increasing maturity: a STXM and TEM study of the Posidonia Shale (Lower Toarcian, northern Germany). Mar. Petrol. Geol. 31 (1), 70–89. https://doi.org/10.1016/j.marpetgeo.2011.05.010.

Bertrand, R., 1990. Correlations among the reflectances of vitrinite, chitinozoans, graptolites and scolecodonts. Org. Geochem. 15 (6), 565–574. https://doi.org/10.1016/0146-6380(90)90102-6.

Borjigin, T., Lu, L., Yu, L., et al., 2021. Formation, preservation and connectivity control of organic pores in shale. Petrol. Explor. Dev. 48 (4), 798–812. https://doi.org/10.1016/S1876-3804(21)60067-8.

Cai, C., Cai, J., Liu, H., et al., 2023. Occurrence of organic matter in argillaceous sediments and rocks and its geological significance: a review. Chem. Geol. 639, 121737. https://doi.org/10.1016/j.chemgeo.2023.121737.

Cao, T., Deng, M., Cao, Q., et al., 2021. Pore formation and evolution of organic-rich shale during the entire hydrocarbon generation process: examination of artificially and naturally matured samples. J. Nat. Gas Sci. Eng. 93, 104020. https://doi.org/10.1016/j.jngse.2021.104020.

Cao, T., Liu, H., Pan, A., et al., 2022. Pore evolution in siliceous shales and its influence on shale gas-bearing capacity in eastern Sichuan-western Hubei, China. J. Petrol. Sci. Eng. 208, 109597. https://doi.org/10.1016/j.petrol.2021.109597.

Chen, J., Xiao, X., 2014. Evolution of nanoporosity in organic-rich shales during thermal maturation. Fuel 129, 173–181. https://doi.org/10.1016/j.fuel.2014.03.058.

Chen, S., Zuo, Z., Moore, T.A., et al., 2018. Nanoscale pore changes in a marine shale: a case study using pyrolysis experiments and nitrogen adsorption. Energy Fuels 32 (9), 9020–9032. https://doi.org/10.1021/acs.energyfuels.8b01405.

Curtis, M.E., Cardott, B.J., Sondergeld, C.H., et al., 2012. Development of organic porosity in the Woodford Shale with increasing thermal maturity. Int. J. Coal Geol. 103, 26–31. https://doi.org/10.1016/j.coal.2012.08.004.

Dong, T., Harris, N.B., McMillan, J.M., et al., 2019. A model for porosity evolution in shale reservoirs: an example from the upper devonian duvernay formation, western Canada sedimentary basin. AAPG Bull. 103 (5), 1017–1044. https://doi.org/10.1306/10261817272.

Gao, Z., Fan, Y., Xuan, Q., et al., 2020. A review of shale pore structure evolution characteristics with increasing thermal maturities. Adv. Geo-Energy Res. 4 (3), 247–259. https://doi.org/10.46690/ager.2020.03.03.

Guo, H., Jia, W., He, R., et al., 2020. Distinct evolution trends of nanometer-scale pores displayed by the pyrolysis of organic matter-rich lacustrine shales: implications for the pore development mechanisms. Mar. Petrol. Geol. 121, 104622. https://doi.org/10.1016/j.marpetgeo.2020.104622.

Hou, L., Ma, W., Luo, X., et al., 2021. Hydrocarbon generation-retention-expulsion mechanism and shale oil producibility of the permian lucaogou shale in the Junggar Basin as simulated by semi-open pyrolysis experiments. Mar. Petrol. Geol. 125, 104880. https://doi.org/10.1016/j.marpetgeo.2020.104880.

Huang, H., Li, M., Yang, C., et al., 2023. A comparison of hydrocarbon generation and expulsion in carbonate and argillaceous source rocks using semi-open pyrolysis experiments. Mar. Petrol. Geol. 155, 106382. https://doi.org/10.1016/j.marpetgeo.2023.106382.

Jarvie, D.M., 2012. Shale resource systems for oil and gas: Part 2—shale-oil resource systems. AAPG Mem. 97, 89–119. https://doi.org/10.1306/13321447M973489.

Jarvie, D.M., Hill, R.J., Ruble, T.E., et al., 2007. Unconventional shale-gas systems: the Mississippian Barnett Shale of north-central Texas as one model for thermogenic shale-gas assessment. AAPG Bull. 91 (4), 475–499. https://doi.org/10.1306/12190606068.

Ko, L.T., Ruppel, S.C., Loucks, R.G., et al., 2018. Pore-types and pore-network evolution in Upper Devonian-Lower Mississippian Woodford and Mississippian Barnett mudstones: insights from laboratory thermal maturation and organic petrology. Int. J. Coal Geol. 190, 3–28. https://doi.org/10.1016/j.coal.2017.10.001.

Kuang, L.C., Hou, L.H., Wu, S.T., et al., 2022. Organic matter occurrence and pore-

forming mechanisms in lacustrine shales in China. Petrol. Sci. 19, 1460–1472. https://doi.org/10.1016/j.petsci.2022.03.005.
Lai, J., Wang, G., Wang, Z., et al., 2018. A review on pore structure characterization in tight sandstones. Earth Sci. Rev. 177, 436–457. https://doi.org/10.1016/j.earscirev.2017.12.003.
Li, K., Zhao, Z., Lu, H., et al., 2022. Effects of inherent pyrite on hydrocarbon generation by thermal pyrolysis: an example of low maturity type-II kerogen from Alum shale formation, Sweden. Fuel 312, 122865. https://doi.org/10.1016/j.fuel.2021.122865.
Liu, B., Mastalerz, M., Schieber, J., 2022a. SEM petrography of dispersed organic matter in black shales: a review. Earth Sci. Rev. 224, 103874. https://doi.org/10.1016/j.earscirev.2021.103874.
Liu, J., Liu, T., Liu, H., et al., 2021. Overpressure caused by hydrocarbon generation in the organic-rich shales of the Ordos Basin. Mar. Petrol. Geol. 134, 105349. https://doi.org/10.1016/j.marpetgeo.2021.105349.
Liu, W., Borjigin, T., Wang, X., et al., 2017. New knowledge of hydrocarbon generating theory of organic matter in Chinese marine carbonates. Petrol. Explor. Dev. 44 (1), 159–169. https://doi.org/10.1016/S1876-3804(17)30020-4.
Liu, X.P., Guan, M., Jin, Z.J., et al., 2022b. Pore structure evolution of lacustrine organic-rich shale from the second member of the Kongdian formation in the Cangdong Sag, Bohai Bay Basin, China. Petrol. Sci. 19 (4), 459–471. https://doi.org/10.1016/j.petsci.2021.12.010.
Löhr, S.C., Baruch, E.T., Hall, P.A., et al., 2015. Is organic pore development in gas shales influenced by the primary porosity and structure of thermally immature organic matter? Org. Geochem. 87, 119–132. https://doi.org/10.1016/j.orggeochem.2015.07.010.
Loucks, R.G., Reed, R.M., 2014. Scanning-electron-microscope petrographic evidence for distinguishing organic-matter pores associated with depositional organic matter versus migrated organic matter in mudrocks. GCAGS J. 3, 51–60. https://www.researchgate.net/publication/273258423.
Loucks, R.G., Reed, R.M., Ruppel, S.C., et al., 2012. Spectrum of pore types and networks in mudrocks and a descriptive classification for matrix-related mudrock pores. AAPG Bull. 96 (6), 1071–1098. https://doi.org/10.1306/08171111061.
Ma, X., Zheng, J., Zheng, G., et al., 2016. Influence of pyrite on hydrocarbon generation during pyrolysis of type-III kerogen. Fuel 167, 329–336. https://doi.org/10.1016/j.fuel.2015.11.069.
Ma, Z., Tan, J., Zhao, H.Z., et al., 2020. Organic geochemistry and geological significance of oil seepage from the Devonian of Luquan area, Yunnan Provine. J. Geomechanics 26 (6), 952–960. https://doi.org/10.12090/j.issn.1006-6616.2020.26.06.076 (in Chinese).
Ma, Z., Tan, J., Zheng, L., et al., 2022. Simulation experiment of fluid-feldspar sandstone interactions and their implications for tight oil and gas exploration of the Yanchang Formation, Ordos Basin. China. Mar. Petrol. Geol. 142, 105737. https://doi.org/10.1016/j.marpetgeo.2022.105737.
Ma, Z., Tan, J., Zheng, L., Shen, B., et al., 2021. Evaluating gas generation and preservation of the Wufeng-Longmaxi Formation shale in southeastern Sichuan Basin, China: implications from semiclosed hydrous pyrolysis. Mar. Petrol. Geol. 129, 105102. https://doi.org/10.1016/j.marpetgeo.2021.105102.
Ma, Z., Zheng, L., Xu, X., et al., 2017. Thermal simulation experiment on the formation and evolution of organic pores in organic-rich shale. Acta Pet. Sin. 38 (1), 23–30. https://doi.org/10.7623/syxb201701003 (in Chinese).
Mastalerz, M., Schimmelmann, A., Drobniak, A., et al., 2013. Porosity of Devonian and Mississippian New Albany Shale across a maturation gradient: insights from organic petrology', gas adsorption, and mercury intrusion. AAPG Bull. 97 (10), 1621–1643. https://doi.org/10.1306/04011312194.
Milliken, K.L., Rudnicki, M., Awwiller, D.N., et al., 2013. Organic matter-hosted pore system, marcellus formation (devonian), Pennsylvania. AAPG Bull. 97 (2), 177–200. https://doi.org/10.1306/07231212048.
Qin, X., Xia, Y., Wu, J., et al., 2022. Influence of pore morphology on permeability through digital rock modeling: new insights from the euler number and shape factor. Energy Fuels 36 (14), 7519–7530. https://doi.org/10.1021/acs.energyfuels.2c01359.
Qiu, N., Chang, J., Zhu, C., et al., 2022. Thermal regime of sedimentary basins in the tarim, upper yangtze and north China cratons, China. Earth Sci. Rev. 224, 103884. https://doi.org/10.1016/j.earscirev.2021.103884.
Ren, D., Zhou, D., Liu, D., et al., 2019. Formation mechanism of the upper triassic yanchang Formation tight sandstone reservoir in ordos basin—take chang 6 reservoir in jiyuan oil field as an example. J. Petrol. Sci. Eng. 178, 497–505. https://doi.org/10.1016/j.petrol.2019.03.021.
Sarmiento, M.F., Rouzaud, J.N., Bernard, S., et al., 2014. Evolution of Barnett Shale organic carbon structure and nanostructure with increasing maturation. Org. Geochem. 71, 7–16. https://doi.org/10.1016/j.orggeochem.2014.03.008.
Shao, D., Zhang, T., Ko, L.T., et al., 2020. Experimental investigation of oil generation, retention, and expulsion within Type II kerogen-dominated marine shales: insights from gold-tube nonhydrous pyrolysis of Barnett and Woodford Shales using miniature core plugs. Int. J. Coal Geol. 217, 103337. https://doi.org/10.1016/j.coal.2019.103337.
Sing, K.S.W., Everett, D.H., Haul, R.A.W., et al., 1985. Reporting physisorption data for gas/solid systems with special reference to the determination of surface area and porosity. Pure Appl. Chem. 57 (4), 603–619. https://doi.org/10.1351/pac198557040603.
Song, D., Tuo, J., Dai, S., et al., 2022. New insights into the role of system sealing capacity in shale evolution under conditions analogous to geology: implications for nanopore evolution. Mar. Petrol. Geol. 143, 105831. https://doi.org/10.1016/j.marpetgeo.2022.105831.
Song, D., Tuo, J., Wu, C., et al., 2020a. Comparison of pore evolution for a Mesoproterozoic marine shale and a Triassic terrestrial mudstone during artificial maturation experiments. J. Nat. Gas Sci. Eng. 75, 103153. https://doi.org/10.1016/j.jngse.2020.103153.
Song, D., Tuo, J., Zhang, M., et al., 2019. Hydrocarbon generation potential and evolution of pore characteristics of Mesoproterozoic shales in north China: results from semi-closed pyrolysis experiments. J. Nat. Gas Sci. Eng. 62, 171–183. https://doi.org/10.1016/j.jngse.2018.12.011.
Song, Y., Gao, F., Tang, X., et al., 2020b. Influencing factors of pore structure differences between marine and terrestrial shale reservoirs. Acta Pet. Sin. 41 (12), 1501–1512. https://doi.org/10.7623/syxb202012005 (in Chinese).
Su, C., Li, R., Shi, G., et al., 2021. Reservoir characteristics of the first member of Middle Permian Maokou Formation in Sichuan Basin and its periphery and inspirations to petroleum exploration, SW China. Petrol. Explor. Dev. 48 (6), 1329–1340. https://doi.org/10.1016/S1876-3804(21)60290-2.
Wang, F., Guo, S., 2019. Influential factors and model of shale pore evolution: a case study of a continental shale from the Ordos Basin. Mar. Petrol. Geol. 102, 271–282. https://doi.org/10.1016/j.marpetgeo.2018.12.045.
Wang, G., Jin, Z., Zhang, Q., et al., 2023a. Effects of clay minerals and organic matter on pore evolution of the early mature lacustrine shale in the Ordos Basin, China. J. Asian Earth Sci. 246, 105516. https://doi.org/10.1016/j.jseaes.2022.105516.
Wang, J.Y., Guo, S.B., 2021. Study on the relationship between hydrocarbon generation and pore evolution in continental shale from the Ordos Basin, China. Petrol. Sci. 18, 1305–1322. https://doi.org/10.1016/j.petsci.2021.01.002.
Wang, Q., Liu, W., Pei, L., et al., 2021. Hydrocarbon generation from calcium stearate: insights from closed-system pyrolysis. Mar. Petrol. Geol. 126, 104923. https://doi.org/10.1016/j.marpetgeo.2021.104923.
Wang, Z., Xin, Y., Xie, W., et al., 2023b. Petroleum geology of marl in triassic Leikoupo Formation and discovery significance of well Chongtan1 in central Sichuan Basin, SW China. Petrol. Explor. Dev. 50 (5), 1092–1104. https://doi.org/10.1016/S1876-3804(23)60451-3.
Wang, Z.H., Ma, Z.L., Zheng, L.J., et al., 2023c. Dynamic evolution characteristics of the “source-reservoir” integration of gray marl and its geological significance to unconventional gas: insights from pyrolysis experiments. Petrol. Sci. 20, 705–720. https://doi.org/10.1016/j.petsci.2023.01.004.
Wu, S., Yang, Z., Zhai, X., et al., 2019. An experimental study of organic matter, minerals and porosity evolution in shales within high-temperature and high-pressure constraints. Mar. Petrol. Geol. 102, 377–390. https://doi.org/10.1016/j.marpetgeo.2018.12.014.
Xia, L.W., Cao, J., Wang, M., et al., 2019. A review of carbonates as hydrocarbon source rocks: basic geochemistry and oil–gas generation. Petrol. Sci. 16, 713–728. https://doi.org/10.1007/s12182-019-0343-5.
Xu, L., Yang, K., Wei, H., et al., 2021. Diagenetic evolution sequence and pore evolution model of Mesoproterozoic Xiamaling organic-rich shale in Zhangjiakou, Hebei, based on pyrolysis simulation experiments. Mar. Petrol. Geol. 132, 105233. https://doi.org/10.1016/j.marpetgeo.2021.105233.
Yang, Y., Liu, X., Zhang, C., et al., 2019. A review and research on comprehensive characterization of microscopic shale gas reservoir space. China Geol. 2 (4), 541–556. https://doi.org/10.31035/cg2018116.
Zhang, Y., Hu, S., Shen, C., et al., 2022. Factors influencing the evolution of shale pores in enclosed and semi-enclosed thermal simulation experiments, Permian Lucaogou Formation, Santanghu Basin. China. Mar. Petrol. Geol. 135, 105421. https://doi.org/10.1016/j.marpetgeo.2021.105421.
Zhu, H., Ju, Y., Huang, C., et al., 2020. Microcosmic gas adsorption mechanism on clay-organic nanocomposites in a marine shale. Energy 197, 117256. https://doi.org/10.1016/j.energy.2020.117256.
Zou, C., Yang, Z., He, D., et al., 2018. Theory, technology and prospects of conventional and unconventional natural gas. Petrol. Explor. Dev. 45 (4), 604–618. https://doi.org/10.1016/S1876-3804(18)30066-1.